ELSEVIER

Tectonophysics 340 (2001) 141–172

TECTONOPHYSICS

www.elsevier.com/locate/tecto

Fluid flow in cataclastic thrust fault zones in sandstones, Sub-Andean Zone, southern Bolivia

Pierre Labaume [a,*], Simon M.F. Sheppard [b], Isabelle Moretti [c]

[a] *Laboratoire de Géophysique Interne et Tectonophysique, Université Joseph Fourier–CNRS, BP 53, 38041 Grenoble Cedex 9, France*
[b] *Laboratoire de Sciences de la Terre, Ecole Normale Supérieure de Lyon–CNRS, 46 Allée d'Italie, 69364 Lyon Cedex 07, France*
[c] *Insitut Français de Pétrole, 1–4 avenue de Bois-Préau, 92852 Rueil–Malmaison, France*

Received 12 July 2000; accepted 18 June 2001

Abstract

The Bolivian Sub-Andean Zone (SAZ) corresponds to a Neogene thrust system that affects an about 10-km thick Palaeozoic to Neogene siliciclastic succession. The analysis of macro and microstructures and cement distribution in thrust fault zones shows that they are sealed by quartz at depths $> \sim 3$ km, due to local silica transfer by pressure-solution/precipitation activated at temperatures >70–90 °C. At shallower depths, faults have remained open and could be preferential drains for lateral flow of carbonate-bearing fluids, as shown by the occurrence of carbonate cements in fractures and their host-sandstone. Due to decreasing burial, resulting from foothill erosion during fault activity, critically buried fault segments can be affected by non-quartz-sealed structures that post-date initial quartz-sealed structures. The integration of textural, fluid inclusion and isotopic data shows that carbonates precipitated at shallow depth (< 3 km), low temperature (< 80 °C) and relatively late during the thrusting history. Isotopic data also show that precipitation occurred from the mixing of gravity-driven meteoric water with deeper formation water bearing carbonate carbon derived from the maturation of hydrocarbon source rocks (Silurian and Devonian shales). The combined microstructural and isotopic analyses indicate that: (i) fluid flow in fault zones often occurred with successive pulses derived from different or evolving sources and probably related to episodic fault activity, and (ii) at a large-scale, the faults have a low transverse permeability and they separate thrust sheets with different fluid histories.

Keywords: Fault zone; Cataclasis; Cement; Fluid flow; Carbon and oxygen isotopes; Bolivia

1. Introduction

Fault zones can be preferential pathways or seals for fluid flow and understanding the factors which control this dual behaviour is crucial to predict the distribution of fluids in faulted domains. Two main types of factors affect fault permeability: (1) the permeability contrasts between country rocks juxtaposed by fault movement and (2) the textural changes related to deformation that modify the permeability of fault zone rocks and adjacent country rocks (e.g., Fisher and Knipe, 1998). These textural changes involve complex interplays between both transient (syn-deformation) and persistent mechanical effects

* Corresponding author. Present address: Laboratoire de Géophysique, Tectonique et Sédimentologic, Université Montpellier II–CNRS, Place E. Bataillon, 34095 Montpellier Cedex 5, France.
E-mail addresses: pierre.labaume@dstu.univ-montp2.fr (P. Labaume), simon.sheppard@geologie.ens-lyon.fr (S.M.F. Sheppard), isabelle.moretti@ifp.fr (I. Moretti).

0040-1951/01/$ - see front matter
PII: S0040-1951(01)00144-5

(fracturing, compaction, dilation) and fluid–rock interactions (dissolution, cementation, mineralogical transformations). To determine their characteristics is an important step for the use of a new generation of numerical models that allow specific hydraulic parameters (thickness, permeability) to be attributed to fault zones (Moretti, 1998; Schneider et al., 1999).

Our work aimed to determine the factors controlling fault zone permeability in the case of thrust faults affecting a mainly silicilastic succession. The study was realised in the Sub-Andean Zone (SAZ) of southern Bolivia, where the capacity of some thrust faults to conduct present-day fluid flow is suggested by the frequent occurrence of oil seeps along fault outcrops (Labaume and Moretti, 1997), whereas other faults seal hydrocarbon accumulations at depth. In a separate paper (Labaume and Moretti, 2001), we show that paleo- and present-day fault zone hydraulic behaviour is primarily controlled by diagenetic conditions at the time of deformation. Specifically, fractures in fault zones are sealed by quartz precipitation activated by temperature at depths exceeding about 3 km, whereas fractures in the shallow part of fault zones remained unsealed. In the present paper, we focus on the relationships between fault zone structure and distribution and characteristics of carbonate (locally, gypsum) cements, which are the main products of paleo-fluid flows in the SAZ. Integrating the textural, mineralogical and carbon and oxygen isotope data of carbonates allows us to discuss the origin and degree of homogeneity of fluid flow both in time and space, at the scale of individual fault zones and at the scale of thrust sheets.

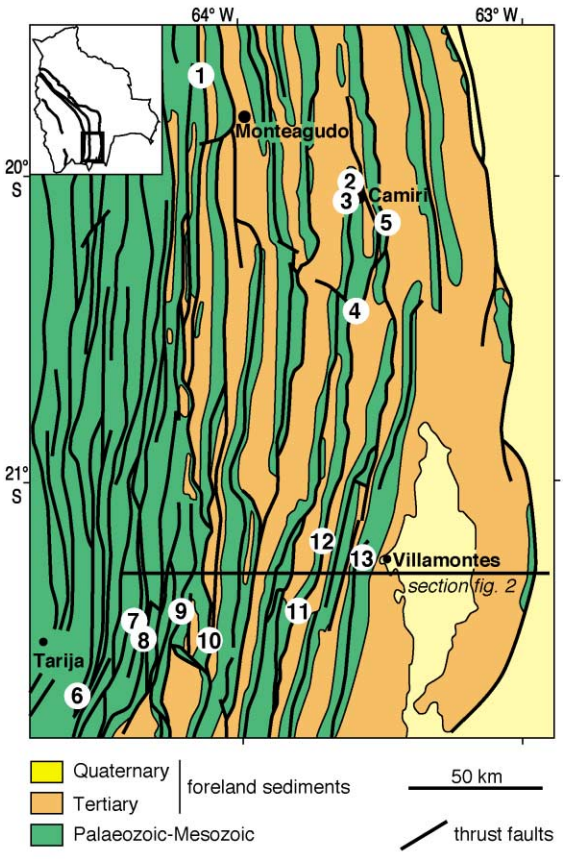

Fig. 1. Structural map of the south Sub-Andean Zone, with location of the studied structures (numbers). 1: Rio Azero fault; 2: Upper Camiri fault; 3: Lower Camiri fault; 4: Cuevo fault; 5: Carohuaicho fault; 6: Tunal fault; 7: Piedra Larga fault; 8: Canaletas fault; 9: Honduras well fault; 10: Pajonal fault; 11: Palos Blancos fault; 12: Rio Pilcomayo fault; 13: Aguarague fault + anticline hinge zone. All structures were studied in outcrops, except the Honduras well fault studied on cores recovered around 2450-m depth. Inset: outline of Bolivia, with Andean belt main thrusts and location of the study area (frame).

2. Geological setting

The SAZ is a Neogene east-verging thrust system that constitutes the eastern border of the Andes (Figs. 1 and 2). The SAZ stratigraphy comprises a thick, mainly siliciclastic Palaeozoic to Quaternary succession resting above a Precambrian basement (Sempere, 1995). In southern Bolivia, the thrust system involves the approximately 10 km thick Silurian to Quaternary succession, which comprises Palaeozoic and Mesozoic platform sediments at the base and the Neogene foreland deposits at the top. The lower part of the Palaeozoic succession is marine, with about 4 km of Silurian–Devonian alternating sandstones and shales passing upward to about 2 km of Carboniferous sandstones. The overlying sediments are mainly continental, with a few hundred metres of Lower Permian fluvial–eolian sandstones, a few tens of metres of evaporitic Upper Permian carbonates and Lower Triassic anhydrite/gypsum and about 1 km of Upper Triassic to Cretaceous fluvial and eolian sandstones. The Upper Cretaceous–Paleogene are reduced to paleosoils, covered by the fluvial Neogene foreland

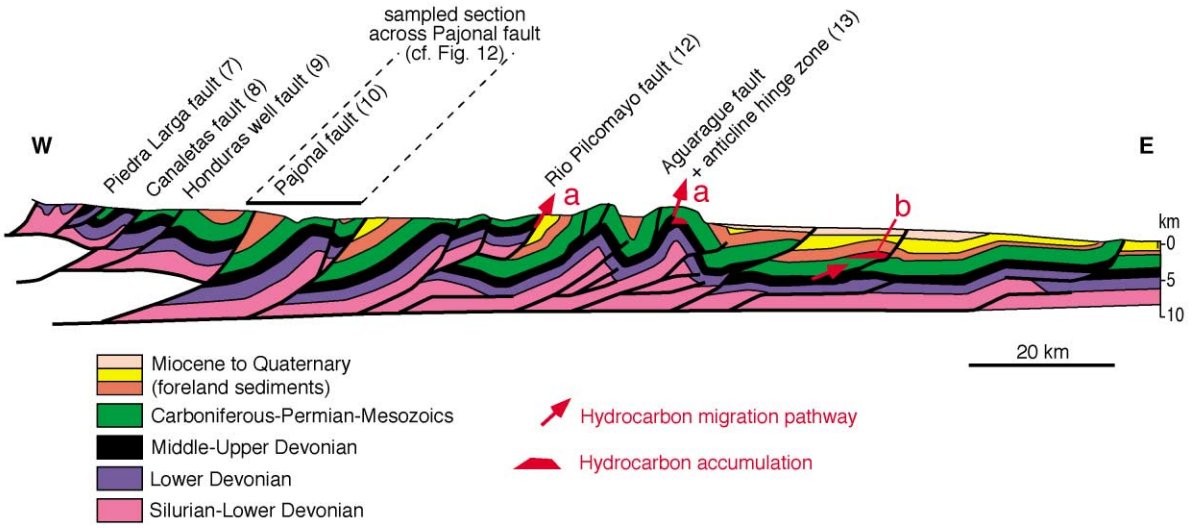

Fig. 2. Structural cross-section of the south Sub-Andean Zone, showing part of the studied structures (location of section and structures in Fig. 1; modified from Moretti et al., 1996; Colletta et al., 1999). (a) Oil seep on fault outcrop; (b) Hydrocarbon trap closure on fault.

sediments. Paleothermometry data derived from analyses of hydrocarbon maturity and apatite fission tracks in sandstones show that the foreland succession commonly reached up to 3 km thick, but early anticlines were less buried (Moretti et al., 1996). The current foredeep succession is around 3.5 km thick in the studied area.

The SAZ development started during the late Oligocene and implies an eastward propagation of the thrust system (Baby et al., 1993; Gubbels et al., 1993; Moretti et al., 1996). In the study area, the deformation is very recent and mainly developed between 6 Ma and the present. The main décollement is located in Silurian shales. The main thrusts have an average spacing of 25 km with a displacement of up to 20 km. Thrust ramp anticlines are associated with most hanging wall ramps and they often feature minor reverse faults related to secondary detachments in the Devonian and Carboniferous shaly intervals. In the inner part of the SAZ, the basement is also involved in the deformation (Kley et al., 1996).

In the SAZ, the main petroleum system consists of the Silurian and Devonian shales as source rocks and all the sandstone units as reservoirs (Moretti et al., 1995). Most hydrocarbon traps are structural traps in anticlines, but faults can play different roles with regard to hydrocarbon migration. In the foothills, oil seeps are numerous (more than 200 have been reported in the Bolivian SAZ) and about 60% of them leak from thrust outcrops (Labaume and Moretti, 1997), showing the capacity of these faults to conduct fluid flow (a in Fig. 2). By contrast, the buried faults in the current foredeep act as efficient seals for hydrocarbon traps on blind anticlines (b in Fig. 2).

3. Faults selected and methods of study

We studied nine large thrusts (Rio Azero, Cuevo, Carohuaicho, Piedra Larga, Canaletas, Honduras, Pajonal, Palos Blancos, Rio Pilcomayo), one back-thrust (Tunal), three minor reverse faults in anticlines (Upper and Lower Camiri, Aguarague) and one fold/fracture zone at an anticline hinge (Aguarague) (Figs. 1 and 2). All structures were studied in outcrops, except the Honduras fault that was studied on well cores recovered at about 2450 m depth. The stratigraphic superpositions observed on faults are Palaeozoic above Palaeozoic (Upper and Lower Camiri, Piedra Larga, Canaletas, Tunal, Aguarague), Palaeozoic above Triassic (Honduras), Palaeozoic above Tertiary (Rio Azero, Cuevo, Carohuaicho, Palos Blancos, Rio Pilcomayo) and Triassic above Tertiary (Pajonal) (Figs. 3 and 4). Structural restorations constrained by paleothermometry data (Moretti et al., 1996) show that, in the case of the large thrusts, the

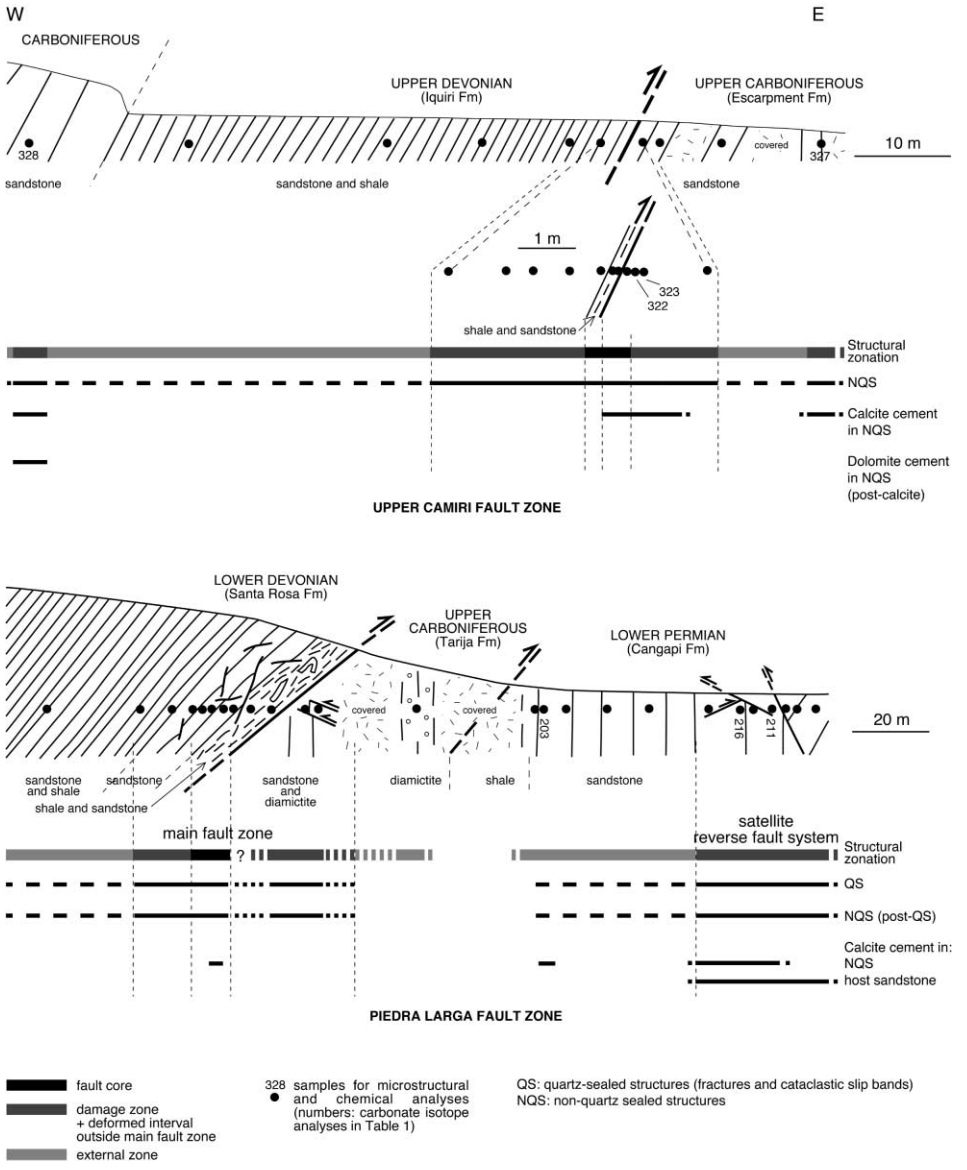

Fig. 3. Sketches of two of the studied fault zones, showing detail of the structural organisation and sampling. The Upper Camiri fault (2 in Fig. 1) features hanging wall and footwall flats. Deformation is dominated by bedding-parallel extension in both compartments. The Piedra Larga fault (7 in Figs. 1 and 2) features a hanging wall flat with a basal detachment in a shale-rich horizon and a footwall ramp. Deformation is dominated by bedding-parallel extension in the hanging wall and horizontal shortening in the footwall. In both cases, note the preferential occurrence of carbonate cements in fault and fracture zones. Some of the dots correspond to several, dm-spaced, samples (total of samples: 35 at Upper Camiri and 51 at Piedra Larga).

burial of the various studied fault-rocks at the beginning of deformation was between a few hundred metres (Tertiary) and up to about 7–8 km (Lower Devonian at Piedra Larga and Canaletas). The depth at the beginning of deformation is less well constrained in the case of the reverse faults in anticlines, because they are late structures that may have begun to form after substantial erosion of anticline crests. Pre-thrust erosion is also possible in the case of the Tunal back-thrust.

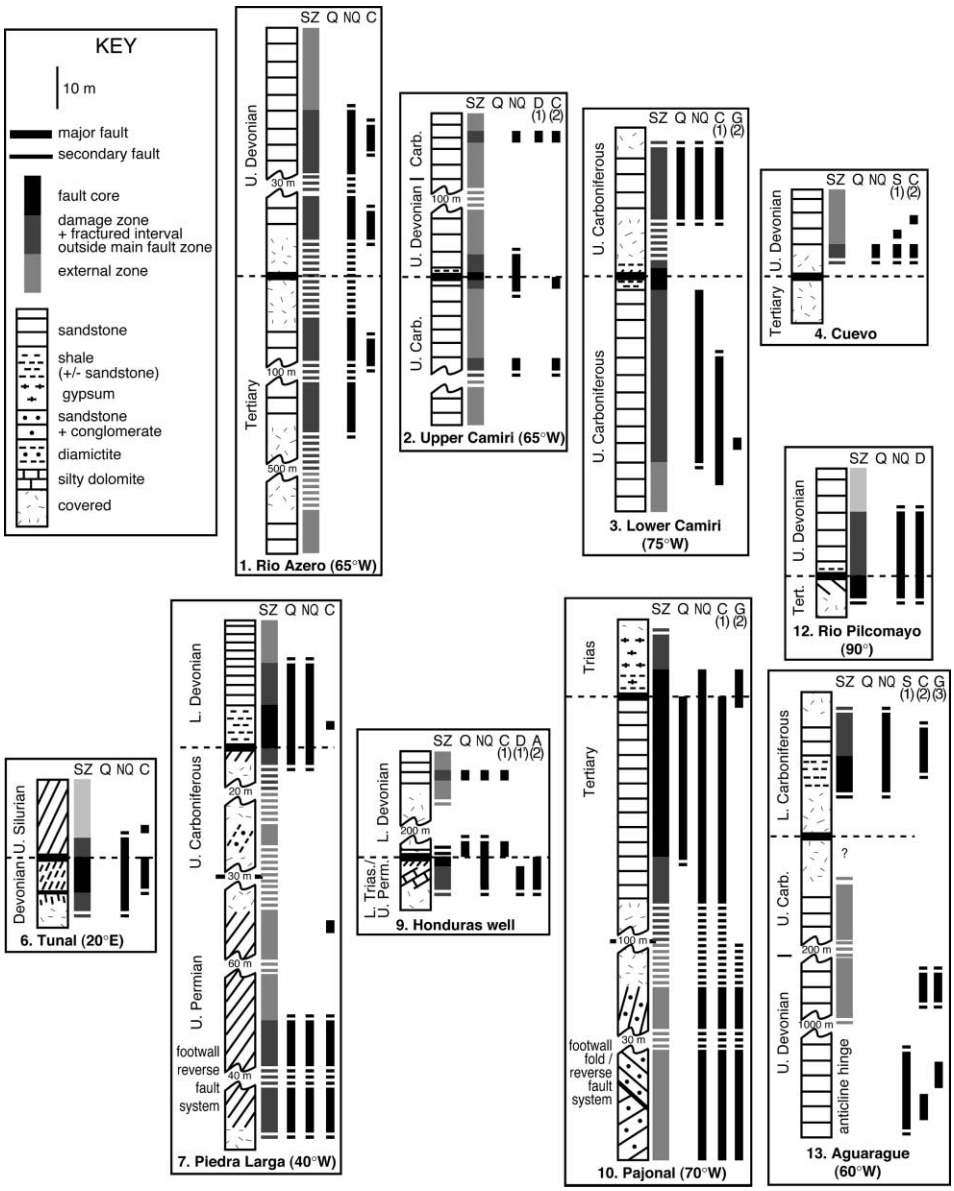

Fig. 4. Structural summary of the studied fault zones (fault zone numbers refer to numbers in Figs. 1 and 2). SZ: Structural zonation; Q: quartz-sealed structures (cataclastic slip bands and fractures); NQ: non-quartz-sealed structures (always posterior to Q); A, C, D, G, S: anhydrite, calcite, dolomite, gypsum and Mg-siderite cements in NQ, respectively (numbers indicate cement chronology). Occasional Q and NQ present in the external zones are not represented. On the other hand, the actual occurrence or absence of carbonate and sulphate cements is represented both inside and outside fault zones. For sketching simplification, the fault contacts are drawn horizontal, their actual dips being indicated below the columns, but the actual fault/bed angular relationships are represented to differentiate fault flats and ramps.

For each fault, a structural analysis was carried out along a profile of a few tens to hundreds of metres across the fault, in order to identify the types and distribution of fault-related deformation structures and mineral veins (Fig. 3). Representative samples of these features and their host-rocks were collected, as well as samples of country rocks located outside (up to a few hundred metres from) the zones affected by

fault deformation to use as reference material. In order to assess the characteristics of background diagenesis, deformation and fluid flow in thrust sheets far from faults, a 20-km-long profile comprising Upper Carboniferous to Tertiary formations was sampled across the Pajonal fault (Fig. 2).

Thin sections of approximately 250 samples were examined using petrographic and scanning electron microscopes (SEM) for petrographic and microstructural study. The SEM was coupled with an energy-dispersive system (EDS) for qualitative and semi-quantitative chemical analyses and hence to determine the mineralogy. Cathodoluminescence (CL) of carbonates was studied with a cold cathode system on a petrographic microscope and CL of quartz was studied with a SEM. These techniques were applied to determine the paragenesis of cements—quartz, carbonate and anhydrite/gypsum. Porosity was measured by microscope image analysis and in a few Devonian samples by the mercury injection technique.

The carbon ($^{13}C/^{12}C$) and oxygen ($^{18}O/^{16}O$) isotope compositions of 102 carbonate samples were analysed from 87 different rock samples representing all the studied fault zones and stratigraphic formations featuring carbonates. Carbonates are only present as minor (few percent) to trace (< 1%) constituents and are difficult to separate physically. Therefore, most isotope analyses were realised on whole rock powders, including samples containing several generations and/or occurrences (i.e., matrix and fractures) of cements. However, in some cases, veins were large enough to allow the preparation of vein and matrix concentrates that were analysed separately. Because carbonates with different mineralogies and chemistries react at different rates during the phosphoric acid (100%) extraction procedures, a few samples of associated carbonates (calcite/dolomite, calcite/Mg-siderite) were chemically semi-quantitatively separated (Epstein et al., 1964; Rosenbaum and Sheppard, 1986). All isotopic data are expressed in the δ-notation as per mil (‰) deviations from standards, PDB for $^{13}C/^{12}C$ ratios and SMOW for $^{18}O/^{16}O$ ratios, using the appropriate CO_2-carbonate fractionation factors (Sharma and Clayton, 1965; Rosenbaum and Sheppard, 1986). For NBS 18, $\delta^{13}C = -5.01‰$ PDB and $\delta^{18}O = 7.15‰$ SMOW ($-23.00‰$ PDB). Precision was better than 0.1‰ for both carbon and oxygen.

Fluid inclusions were examined in carbonate and quartz cements both within and outside of fault zones, to set limits on temperatures of cementation. Although fluid inclusions are present in carbonates, they are overwhelmingly both very small in diameter (< 2 μm) and monophase (aqueous) inclusions. The very rare biphase inclusions observed were usually close to the edge of the crystal. They thus probably have undergone leakage and are not considered further. Inclusions in quartz cements were also too small to study by standard microthermometric methods.

4. Macrostructure of fault zones

At the scale of the studied outcrops, the angular relationships between fault surface and bedding define either flats or ramps (Figs. 3 and 4). In all cases, sandstone is the most frequent lithology affected by the fault-related deformation. However, several faults feature a hanging wall flat along a few dm- to m-thick hanging wall detachment horizon made of alternating shale and sandstone beds (Upper and Lower Camiri, Piedra Larga, Canaletas, Rio Pilcomayo, Aguarague) or shale and gypsum beds (Pajonal). Other shaly horizons occur in the footwall at Tunal, Lower Camiri and Honduras. In the latter case, the shale contains anhydrite lenses and overlies silty dolomite.

Fault-related deformation structures are distributed over a few metres to tens of metres on both sides of the fault surface (Fig. 5). We define this band of deformed rocks as the ''fault zone'', qualitatively differentiated into a fault core with strong deformation and highly disturbed bedding and peripheral damage zones with weaker deformation and globally preserved bedding (Caine et al., 1996) (Figs. 3 and 4). Fault zone thickness varies from about 10 m at Upper Camiri, a minor reverse fault (offset about 1 km), to more than 200 m at Rio Azero, a large thrust (offset about 20 km) (Fig. 4). However, most fault zones are about 20–50 m thick, without a clear relationship between fault zone thickness and fault offset. Fault-related deformed intervals can also occur outside (up to a few hundred metres from) the main fault zone. In the following, the term ''fault zone'' also includes these deformed intervals.

In sandstones, the characteristic structures are cataclastic slip bands and shear or extension fractures

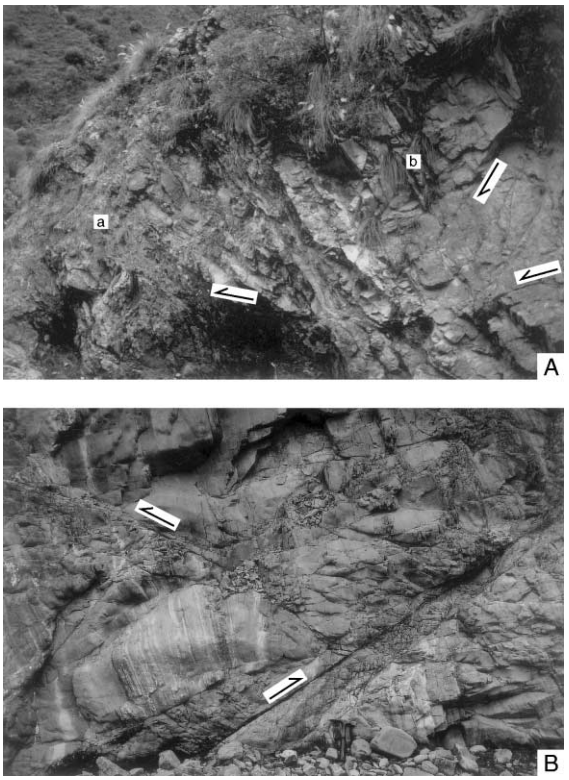

Fig. 5. Outcrop aspect of fault zone deformation. (A) Canaletas fault zone. Hanging wall beds (Lower Devonian Santa Rosa Fm) dip 40°W, parallel to the fault surface (located about 1 m left of the left photograph side). The fault features a basal detachment in a 10-m thick disrupted shale-rich interval (fault core, a) passing upwards to fractured sandstone beds (damage zone, b). The deformation corresponds to bedding-normal extension, with bedding-normal extension fractures and oblique shear surfaces (arrows) which flatten in the shale layers. View is about 12 m wide. (B) Satellite reverse fault system in the Piedra Larga fault footwall (Lower Permian Cangapi Fm; cf. Fig. 3). Beds are sub-vertical and are cut by a network of mm-thick cataclastic slip bands with mm- to dm-offsets (arrows) corresponding to horizontal shortening. View is about 4 m wide.

(Fig. 5), all possibly featuring quartz, carbonate or gypsum cementation. Structures have a close (centimetre or less) spacing and a high degree of connectivity in the fault core and these are more widely spaced and less connected in the damage zones. In alternating shales–sandstones (or shales–gypsum/anhydrite), deformation consists of boudinage of the sandstone layers (or gypsum/anhydrite) into cm- to m-scale lenses and scaly fabric and microfolding of the shaly matrix (Fig. 5A). Where shaly detachment horizons are present, they concentrated the deformation and hence correspond to the fault cores, whereas the adjacent more competent sandstones (silty dolomite at Honduras) are less deformed and correspond to the damage zones. The deformation kinematics in fault zones are complex. However, we could observe that deformation corresponds mainly to bedding-parallel extension in the hanging wall detachment horizons and to low-dipping compression in the footwall ramps (Figs. 3 and 5).

5. Sandstone petrology

In all formations, the sandstones are subarkosic, with 70–80% of quartz grains and 10–20% of alkali feldspar grains. They can also contain up to a few percent of clay and micas and occasional rock fragments and accessory minerals (tourmaline, apatite, zircon). Early quartz cements with chalcedony to macrocrystalline texture locally occur in the Lower Permian sandstones. Carbonate and, to a lesser extent, gypsum cements are sometimes present in both the undeformed and deformed samples. Their occurrences and characteristics are the main topic of this paper and are described in detail in Section 7.

The degree of burial compaction and diagenesis is assessed from the study of samples collected outside fault zones, in order to avoid possible compactional effects related to fault deformation. The matrix porosity is high (up to about 20%) in the upper part of the section. At burial levels of 2.5–3 km, i.e. between the Mesozoic and Upper Carboniferous formations depending on the local thickness of the Tertiary, the onset of chemical compaction occurs. Chemical compaction affects quartz and feldspar grains and is characterised by pressure solution at grain contacts and by mineral overgrowths. It resulted in a drastic reduction of porosity that decreases to less than 5% in most samples below the Upper Carboniferous. This depth-distribution of chemical compaction and its effect on porosity are similar to those observed in other siliciclastic platforms (Bjørlykke and Egeberg, 1993). The depth-dependence of chemical compaction is interpreted as resulting from temperature-control, because the kinetics of dissolution/precipitation of silica only have geologically efficient rates at temperatures $> \sim 80$ °C (Oelkers et al., 1996; Renard et al.,

1999). In the SAZ of southern Bolivia, the average surface temperature is about 15 °C and the geothermal gradient is about 22 °C/km (Moretti et al., 1996; Husson and Moretti, 1999), so the observed depth of the onset of chemical compaction accords with this theoretical limit of temperatures.

Two other common diagenetic features are (i) the partial dissolution of K-feldspar grains, which resulted in the formation of a secondary porosity that can reach several percent in some samples and (ii) the precipitation of kaolin with a book texture. Both features probably represent rather shallow diagenesis related to the circulation of meteoric water (Bjørlykke, 1994). The fact that kaolin is kaolinite in the Upper Carboniferous sandstones at Camiri and dickite in the Devonian sandstones at Piedra Larga and Rio Pilcomayo reflects the kaolinite to dickite conversion during progressive burial (Labaume and Moretti, 2001).

6. Microstructures related to fault-zone deformation in sandstones

Deformation of sandstones in fault zones was dominated by brittle fracturing (cataclastic) processes correlated with the matrix porosity. This relationship indicates that porosity controlled the sandstone's mechanical behaviour at the small scale and that faulting occurred after most of the burial compaction was achieved. Fracturing could be associated, or not, with pressure solution and quartz sealing. These aspects are detailed in a separate paper (Labaume and Moretti, 2001) and are only summarised here.

Porous sandstone fracturing is characterised by intragranular fractures, generated by stress concentrations at the grain contacts that support the grain framework. At the cm-scale, deformation can be distributed with variable patterns and intensity, from domains with a low density of subparallel fractures to completely crushed grains. Localisation of deformation resulted in the concentration of fractures in mm-thick shear zones characterised by strong grain size reduction (Fig. 6A

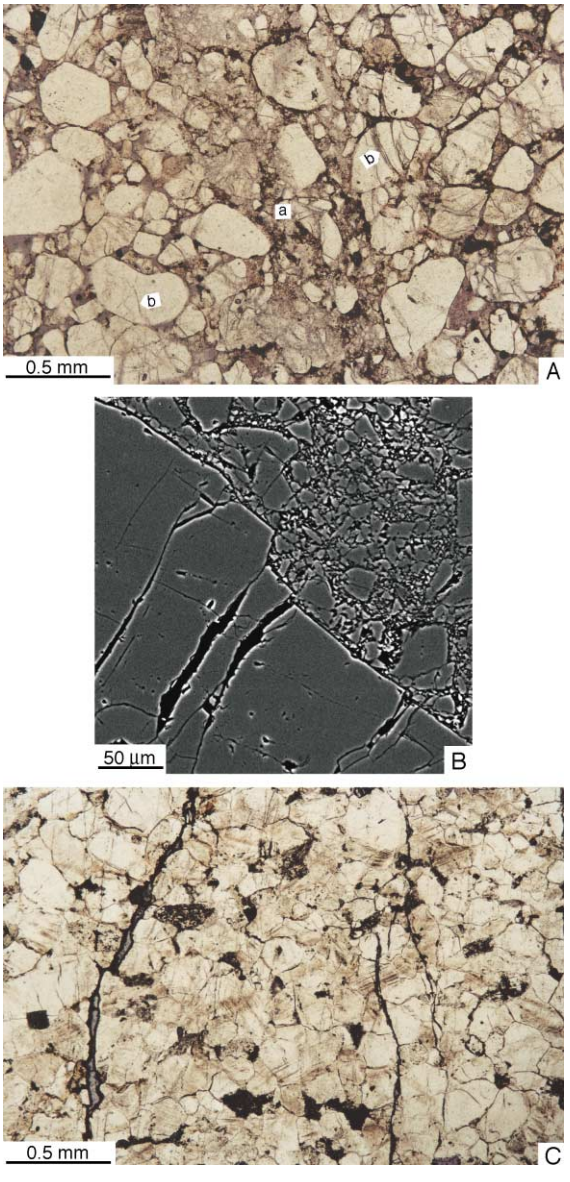

Fig. 6. Fault-related fracturing processes in sandstones in relation to initial porosity. (A) Porous sandstone, cataclastic slip band (CSB; a) and peripheral intragranular fractures (b). Note (i) inside the CSB, the strong reduction of porosity due to mechanical compaction of grain fragments and (ii) at CSB periphery, the intragranular fracture porosity and preserved primary porosity (light violet: impregnation epoxy resin in pores) (Upper Carboniferous Escarpment Fm, Lower Camiri fault footwall; plain light microphotograph). (B) Porous sandstone, detail in a CSB. The lack of quartz sealing resulted in preserved porosity (black) between quartz grain fragments (grey) (Tertiary, Rio Azero fault zone; backscattered SEM image). (C) Low-porosity sandstone, set of transgranular fractures. Note the fracture porosity (blue: impregnation epoxy resin in pores) (Lower Devonian Santa Rosa Fm, Piedra Larga fault zone; plain light microphotograph).

and B). These shear zones are similar to those already described in other examples of faulted porous sandstones (e.g., Aydin and Jonhson, 1983; Antonellini et al., 1994; Fowles and Burley, 1994) and are here referred to as cataclastic slip bands (CSBs), according to the terminology proposed by Fowles and Burley (1994). In most CSBs, offset is very small (millimetric or less) and cohesion was not lost across the band. However, larger offset may have resulted in the formation along the CSB of a discrete striated slip surface. When mineral sealing is lacking, grain fragments in the CSB were mechanically compacted, resulting in a low porosity of the CSB compared to that of the host-sandstone (see also Antonellini and Aydin, 1994; Fowles and Burley, 1994).

Low porosity sandstones had a higher mechanical homogeneity than the porous sandstones, which favoured the formation of transgranular fractures up to several dm long (Fig. 6C). They are extensional or shear fractures and can be grouped in mm-thick Riedel-type shear zones (Tchalenko, 1968). Increasing density of fractures during shear zone development may have resulted in a microstructure analogous to that of the CSBs in porous sandstones. When mineral sealing is lacking, the fracture porosity is high compared to the matrix porosity of the host-sandstone.

Sandstones featuring typical intragranular fracturing have porosities up to around 20% and occur in the upper part of the section, from the Tertiary to the Upper Carboniferous formations, whereas sandstones featuring the typical transgranular fracturing have porosities lower than 5% and occur in the lowermost part (Silurian and Devonian formations). Sandstones with intermediate porosities (5–10%), due to the limited development of chemical compaction, mainly occur from the Lower Permian to the Upper Devonian formations. In these sandstones, fractures are mostly transgranular but they contain many segments that follow weakly cohesive grain contacts rather than cutting the grains and sets of closely spaced fractures frequently evolved into CSBs.

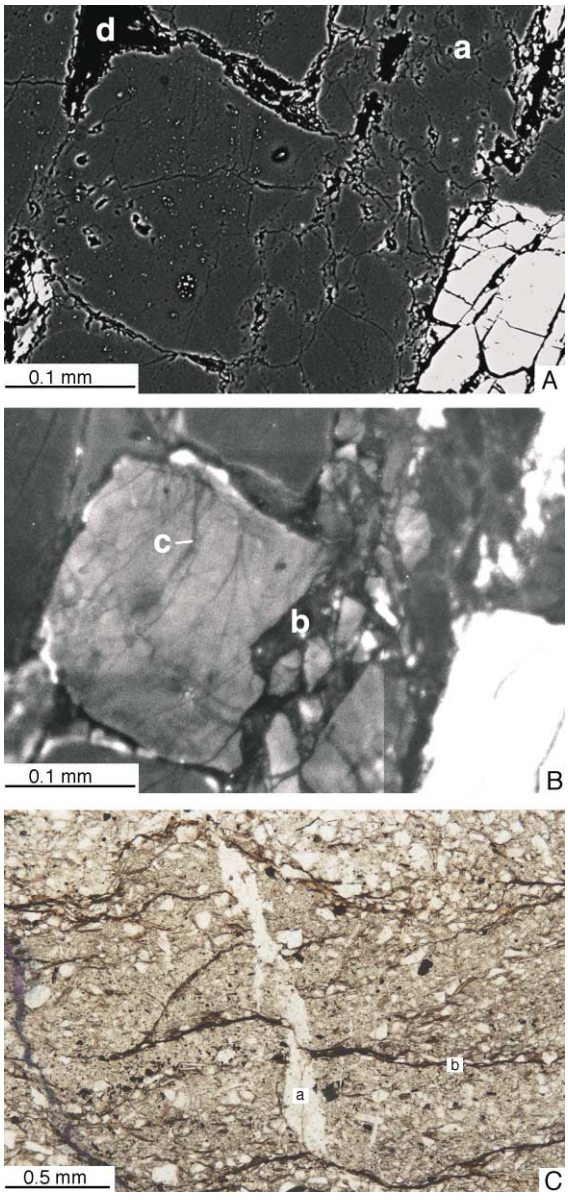

Fig. 7. Quartz-sealing and pressure solution features in cataclastic slip bands (CSBs) and fractures. (A and B) Porous sandstone, quartz-sealed CSB (a) and peripheral zone on back-scattered (A) and cathodoluminescence (B) SEM images. In (A), dark grey is quartz, white is K-feldspar and black is porosity. In (B), authigenic quartz appears in black. It precipitated between grain fragments in the CSB (b) and thin intragranular fractures in the peripheral zone (c). Note the very low porosity in the CSB and preserved intergranular porosity in the peripheral zone (d) (Upper Carboniferous Tarija Fm, Piedra Larga fault zone). (C) Low-porosity sandstone, quartz vein (a) filling a transgranular fracture, associated with pressure solution seams in the host sandstone (b) (Lower Devonian Santa Rosa Fm, Piedra Larga fault zone; plain light microphotograph).

The brittle structures described above may, or may not, be associated with pressure solution structures affecting quartz and feldspar grains and sealing by authigenic quartz. In porous sandstones, quartz-sealing occurs in dilated intragranular fractures both inside and at the periphery of the CSBs (Fig. 7A and B). In many cases, quartz precipitated only in the fractures and not in the pre-existing matrix porosity, probably because nucleation was favoured on the clean fracture surfaces, whereas it was inhibited by clay or oxide coatings on the detrital grain surfaces. Pressure solution can be observed at intergranular contacts both inside and outside CSBs. In low porosity sandstones, quartz sealing of transgranular fractures resulted in the formation of veins up to a few mm thick, often associated with stylolites along mica/clay-rich layers (Fig. 7C). The close association of pressure solution structures and fracture quartz sealing suggests that the authigenic quartz was mainly derived from local dissolution sites and was transported over short distances to the precipitation sites.

Six of the studied fault zones display only non-quartz-sealed structures (Rio Azero, Upper Camiri, Cuevo, Tunal, Rio Pilcomayo, Aguarague) and five display both quartz-sealed and non-quartz-sealed structures (Lower Camiri, Piedra Larga, Canaletas, Honduras, Pajonal) (Fig. 4). Cross-cutting relationships show that the non-quartz-sealed structures always post-date the quartz-sealed ones.

7. Carbonate cements in sandstones

Carbonate occurs in most sandstone formations, both inside and outside of the fault zones and as both matrix and fracture cements, the latter being restricted to the non-quartz-sealed structures. However, although they are widespread, carbonates always occur in small amounts (usually <5 wt.% of whole rock) and with an irregular distribution: many hand specimens are un- or incompletely cemented. Calcite is the most common carbonate, but dolomite and Mg-siderite are locally present. The macroscopic distribution of these different cements is summarised in Fig. 4. In this section, we first summarise the main characteristics of carbonate cement typology, paragenesis and isotopic data, then we show how these features are combined in the different fault zones.

7.1. Typology of carbonate cements at the cm (hand-sample)-scale

Sandstone matrix carbonate cements occur in intergranular pores (Fig. 8A), locally in pre-existing secondary pores resulting from feldspar dissolution, but cementation is rarely complete at the cm-scale, i.e. part of the matrix porosity is generally preserved. Carbonate precipitation was often associated with partial dissolution/replacement of quartz and feldspar grains (Fig. 8B). Carbonate always post-dates the quartz and feldspar overgrowths related to chemical compaction, that can also be affected by the replacement process (Fig. 8B). The latter mechanism was particularly developed in the lower part of the succession where the intergranular porosity was very small, due to strong pre-carbonate chemical compaction (Fig. 8C). These textural characteristics show that carbonate precipitation occurred after sandstone compaction was largely achieved.

The carbonate-cemented CSBs usually contain abundant cement into which the detrital grain fragments appear to float, implying that carbonate precipitation was associated with strong dilation of the cataclastic texture (a in Fig. 9A and B). In some cases, cementation continued with formation of carbonate veinlets in through-going fractures preferentially located at the CSB borders (b in Fig. 9A and B). The carbonate is generally little deformed by twinning. These features indicate that cementation occurred late with respect to quartz grain cataclasis. In only one case (Rio Azero footwall), we observed CSBs containing scarce and intensely twinned calcite crystal aggregates, suggesting that calcite precipitated before or during the early stages of CSB formation. In transgranular shear and extension fractures, carbonate precipitation resulted in the formation of veins up to a few mm thick (Fig. 9E–J). Some of the CSBs and shear veins show carbonate concentration in dilational jogs (Sibson, 1996), sometimes with a fibrous fabric, indicative of precipitation during/immediately after shear movement (Fig. 9C). However, in other cases, we cannot exclude carbonate precipitation during a late, extensional fracture reactivation. Only one extension vein and one shear vein show inclusion bands in carbonate fill indicating episodic opening by a crack-seal mechanism (Ramsay, 1980; Labaume et al., 1991). In both CSBs and veins, cementation is rarely

complete at the cm-scale, i.e. part of the fracture porosity is often preserved, locally with a geodic crystal pattern (Fig. 9G).

Most sandstone samples that contain carbonate-cemented CSBs or veins also contain matrix carbonate cement in the host-sandstone (Fig. 9A–H). In only one case, we observed fractures sealed by calcite cutting a porous host-sandstone that contains almost no carbonate cement (Fig. 9J). Where carbonate-cemented fractures cut older quartz-sealed CSBs, carbonate could also precipitate in the latter through a replacement mechanism and it forms irregular patches secant on the quartz-sealed cataclasite microstructure (Fig. 9C and D).

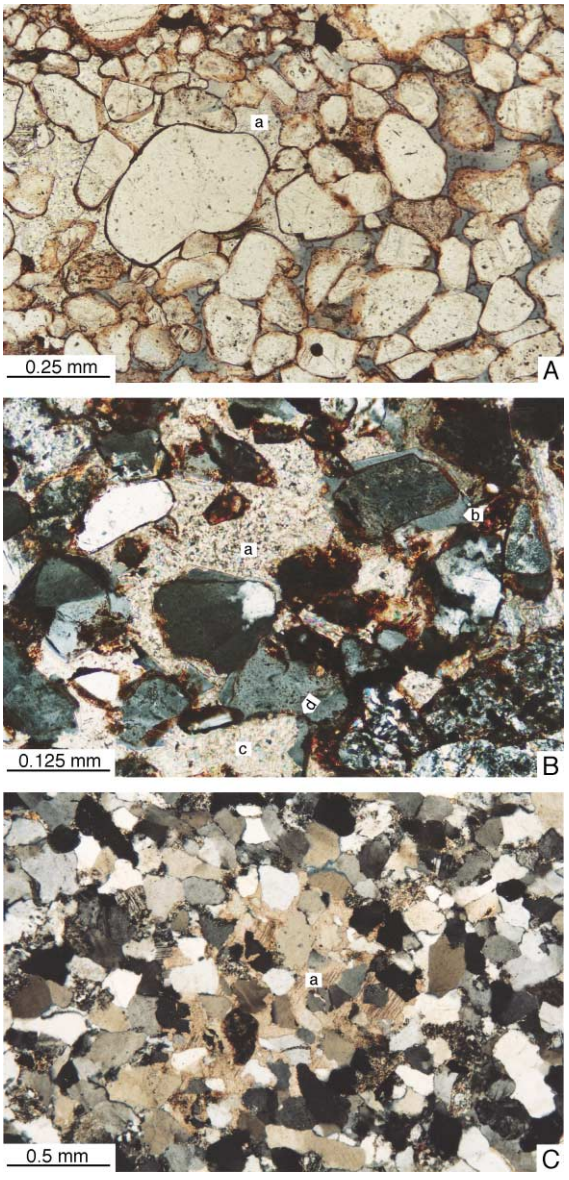

Fig. 8. Matrix carbonate cements in sandstones. (A) Poorly compacted sandstone with calcite cement (a) in intergranular pores. Cementation was incomplete (blue: impregnation epoxy resin in pores) (Jurassic–Cretaceous Ichoa Fm, Pajonal fault footwall; plain light microphotograph). (B) Calcite cement (a) covering (post-dating) quartz overgrowths (b) related to chemical compaction. Calcite precipitated in relation to dissolution/replacement of quartz grains and overgrowths (c). (d) Pressure solution contact related to chemical compaction (Triassic San Diego Fm, Pajonal fault hanging wall; crossed polarisers microphotograph). (C) Patch of poikilotopic calcite cement (a) in low-porosity sandstone. Low porosity is due to strong pre-calcite chemical compaction and calcite precipitation was related to dissolution/replacement of quartz (Lower Devonian Huamampampa Fm, Honduras well fault hanging wall; crossed polarisers microphotograph).

7.2. Mineralogy and paragenesis of carbonate cements

Outside fault zones, carbonates in sandstones occur mostly as matrix cements and are most often calcite. The only exceptions are (i) an Mg-siderite matrix cement in Middle–Upper Devonian sandstones at Cuevo and Aguarague (anticline hinge zone; $Mg/Mg+Fe=0.26–0.48$) and (ii) a dolomite cement in fracture and host-sandstone in a Triassic sample from the Pajonal fault hanging wall. At Cuevo, Mg-siderite is also present in one sample from the fault zone, but it precipitated before fault zone formation (see below, Section 7.4.4).

Inside fault zones, carbonate cements are most often calcite, locally dolomite. Dolomite can be the only carbonate present (Rio Pilcomayo footwall and hanging wall), or occur associated with calcite (Upper Camiri hanging wall). In most cases, the mineralogy and CL characteristics of carbonates are similar in the CSBs or veins and their host-sandstone. This similarity sometimes includes the occurrence of several generations of carbonate, revealed by CL in a monomineralic carbonate (Fig. 9B, F and H) or, in one case, a change of mineralogy (Fig. 9I). These features suggest (i) a coeval precipitation from the same fluid in fractures and host-sandstones and (ii) the possible

occurrence of several episodes of rupture and cementation by fluids of different composition.

7.3. Carbonate cement isotope data

The carbon and oxygen isotope compositions of carbonates from matrix and fracture cements and sedimentary carbonates are presented in Table 1, together with age and nature of the host-rocks. Most cements are from sandstone samples, except two dolomite veins in dolomite host-rock at Honduras. The sedimentary carbonates correspond to seven samples from the Upper Permian/Lower Triassic evaporites (four dolomites, two magnesites and one calcite). The cement data as a whole (Fig. 10) show a very wide range of $\delta^{13}C$ values, from $+1.7‰$ to $-26.1‰$, PDB, and less variable $\delta^{18}O$ values, from 14.3‰ to 26.1‰, SMOW, with one sample at 32.7‰. The dispersion of values for the matrix and fracture cements is very similar to each other. Most of these values are different from the SAZ sedimentary carbonate field (Fig. 10).

The carbonate cements can be divided into three main types of occurrence: (1) fault cores, (2) damage zones and (3) sections external to fault zones. For these three carbonate occurrences, the mean of the mean $\delta^{18}O$ value for each fault is very similar: 20.2‰ for five fault cores, 20.2‰ for 10 damage zones and 20.4‰ for eight sections outside fault zones. The dispersion of the $\delta^{18}O$ values shows no clear relation with stratigraphic formation or structural location. In particular, the Paleozoic and Mesozoic rocks, most of which have had a relatively deep burial history with maximum estimated temperatures between 120 and 200 °C, contain cements with $\delta^{18}O$ values that are indistinguishable from those in Tertiary formations ($<\sim 3$ km deep or <80 °C). However, the most ^{18}O-depleted values ($<\sim 18‰$) are more prevalent in Silurian, Devonian and Carboniferous rocks.

About 2/3 of the complete range of $\delta^{13}C$ values are between $-6‰$ and $-13‰$, in part because of the relatively large number of samples from Pajonal. Values within this more limited range are present at all studied outcrops except Lower Camiri and Carohuaicho. Except for one sample from Honduras, all the $\delta^{13}C$ values $<-13‰$ occur in fault zones of the external (eastern) part of the SAZ (Camiri, Cuevo, Rio

Fig. 9. Carbonate cements in cataclastic slip bands (CSBs) and transgranular fractures in sandstones. (A) Dolomite cement in a CSB (a), late veinlets at CSB periphery (b) and host-sandstone (c). Dolomite precipitation implied strong dilation of the cataclasite, with detrital grain fragments floating in the cement (Tertiary, Pilcomayo fault zone; plain light microphotograph). (B) Detail of (A) (centre bottom) on a cathodoluminescence (CL) microphotograph. There are three main generations of dolomite, the first one bright yellow luminescent at the centre of crystals, the second one red luminescent at the periphery and the third one dull luminescent in late veinlets (b). Each generation features a fine zoning marked by variations of luminescence intensity. The same three generations are also present in the host-sandstone cement (not visible on the photograph). (d) quartz; blue: K-feldspar. (C) Non-quartz-sealed CSB (arrows) cemented by calcite (a) and cutting across an older quartz-sealed cataclasite (b). Calcite cement also forms patches in the older cataclasite ((c); see detail in (D)). Note that calcite in the CSB precipitated in dilated domains with a complex geometry, but two of these domains (a) show a rough-rhomb shaped geometry interpretable in terms of dilational jogs compatible with the shear movement indicated by arrows, arguing for syn-kinematic calcite precipitation (Tertiary, Pajonal fault zone; crossed polarisers microphotograph). (D) Detail in the sample shown in (C). The quartz-sealed cataclasite (a) is post-dated by calcite cement (b) related to neighbouring non-quartz-sealed fractures. Calcite precipitation implied dissolution/replacement of quartz, resulting in calcite patches secant on the quartz-sealed cataclasite texture. (E and F) Plain light (E) and cathodoluminescence ((F), central and left parts of (E)) microphotographs of calcite cement in a transgranular fracture and host sandstone. The vein contains a first generation of bright red luminescent calcite (a) cut by a second-generation veinlet of non-luminescent calcite (b). Calcite of the first generation is also present as a matrix cement in the host-sandstone (c), where it covers (post-dates) quartz overgrowths (d). Vein opening and calcite precipitation post-dates quartz-sealed cataclastic deformation ((e); see more details of similar feature in (C) and (D)). Calcite precipitated in relation to dissolution/replacement of quartz (f) (Carboniferous, Lower Camiri fault zone). (G and H) Plain light (G) and cathodoluminescence (H) microphotographs of dolomite cement in transgranular fractures (a) and host-sandstone (b). The veins in fractures have a geodic texture with cavities partially filled with oxide (c). There are two main generations of dolomite, with the same characteristics as the first two shown in (B). In (H), black is quartz and pores, and blue is K-feldspar (Upper Devonian Iquiri Fm, Pilcomayo fault zone). (I) Transgranular fractures filled with a first generation of dolomite (a) and a second generation of calcite (b) with geodic cavities (black). (c) quartz grain; (d) K-feldspar grain; (e and f) pre-dolomite chlorite and iron oxide cements, respectively (Carboniferous, Upper Camiri fault hanging wall; back-scattered SEM image). (J) Transgranular fracture filled with calcite in a porous sandstone. In this case, calcite precipitated mainly in the fracture (a), whereas it is rare in the host-sandstone (b) whose pores remained mainly uncemented (black). (c) quartz grain; (d) K-feldspar grain (Upper Carboniferous Escarpment Fm, Upper Camiri fault zone; back-scattered SEM image).

Pilcomayo, Aguarague), but all samples from these outcrops are not strongly ^{13}C-depleted. Most of the $\delta^{13}C$ values $< -13‰$, and all those $< -20‰$, occur in Devonian and Carboniferous rocks. A few values $< -13‰$ occur in the Tertiary sandstones located close to (a few metres from) Upper Devonian alternating shales–sandstones (Rio Pilcomayo). Considering the three main types of carbonate occurrences, although the range of values are roughly similar, the mean of the mean values of the different faults increases from external ($-15.0‰$) to damage zone ($-11.9‰$) to fault core ($-9.9‰$).

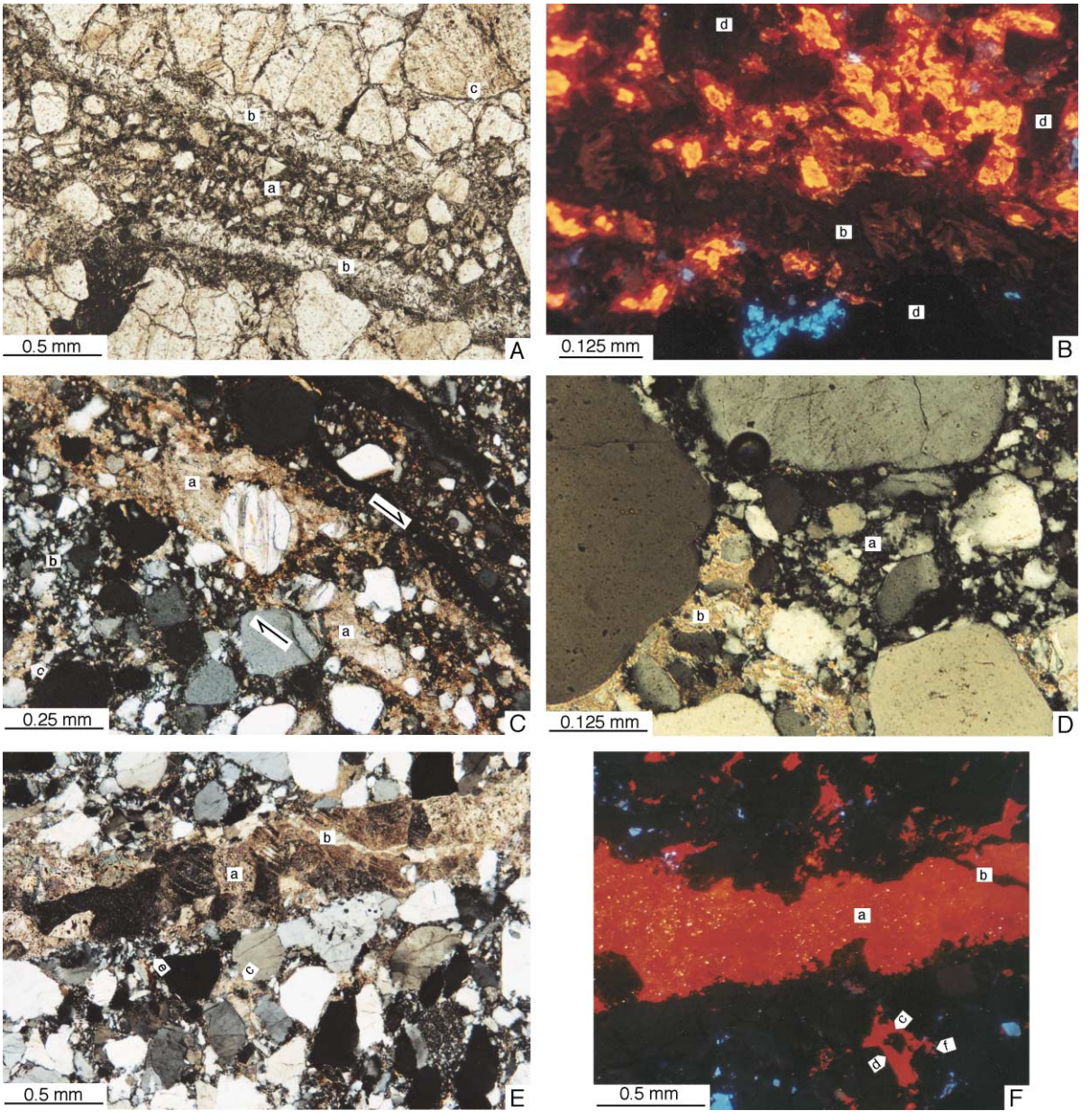

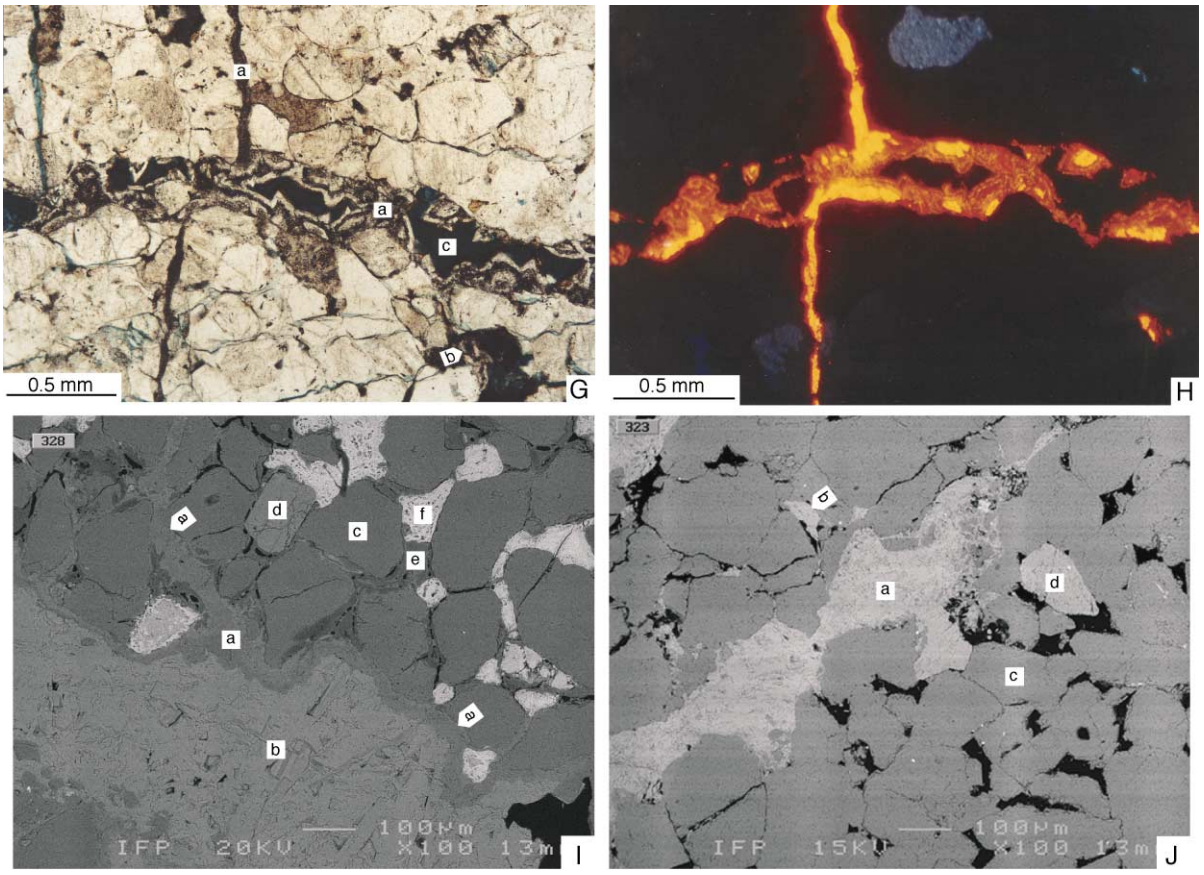

Fig. 9 (*continued*).

7.4. Carbonate cements at the fault zone-scale

The Canaletas fault zone is the only one where no carbonate cement was observed. In all other faults, there is a preferential concentration of carbonate in the inside part of the fault zone, whereas it is absent or scarce in the nearby external zones (i.e., at distances of a few tens of metres from the fault zone) (Figs. 3 and 4). Carbonate can be present in both compartments of the main fault zone or only in one compartment. It can also be concentrated in the deformed intervals located outside the main fault zone. Distribution of carbonate is also heterogeneous at the m-scale: inside a given fault zone compartment, its amount varies greatly from one sample to another and some samples may have no carbonate. Below, we describe the main characteristics of carbonate cementation in each fault zone. We also describe the few occurrences of anhydrite and gypsum cements and their relationships with carbonate cements.

7.4.1. Rio Azero fault (1 in Fig. 1)

The fault places Upper Devonian low-porosity sandstones above Tertiary high porosity sandstones. Calcite cement is present in both damage zones (the fault core is not visible) and absent in the external zones. Its distribution is very heterogeneous (many samples do not contain carbonate), but it is more abundant in the footwall. Calcite occurs in CSBs and host-sandstone in the footwall and in shear veins and host-sandstone in the hanging wall (Fig. 4). In the footwall, calcite is scarce and highly deformed inside the CSBs, whereas it can be abundant in their host-sandstone, with coexisting highly and slightly

Table 1
Oxygen and carbon isotope data of carbonates. Samples are grouped by fault zone section and, in each section, are listed going structurally downwards, with indication of fault zone structural zonation (fault zone numbers refer to numbers in Figs. 1 and 2)

Sample[a]	Carbonate	% Carb.[b]	δ13-C ‰ PDB	δ18-O ‰ PDB	δ18-O ‰ SMOW	Host-rock	Host-rock age	Remarks[c]
1. Rio Azero fault								
Hanging wall, damage zone								
300	calcite	0.9	− 2.92	− 15.60	14.78	sandstone	U. Devonian	matrix
304	calcite	3.4	− 5.59	− 13.05	17.41	sandstone	U. Devonian	matrix
Footwall, damage zone								
295	calcite	5.8	− 9.60	− 14.14	16.28	sandstone	Tertiary	vein + matrix
306	calcite	9.2	− 10.58	− 11.92	18.57	sandstone	Tertiary	vein + matrix
308	calcite	11.9	− 11.86	− 13.42	17.03	sandstone	Tertiary	matrix
2. Upper Camiri fault								
Hanging wall, peripheral fracture zone outside main fault zone								
328	calcite	0.2	− 10.94	− 5.37	25.32	sandstone	Carb.	matrix concentrate, post-dolomite
"	dolomite	0.6	− 14.37	− 5.77	24.91	sandstone	Carb.	matrix concentrate
328va	calcite	3.0	− 11.14	− 7.17	23.47	sandstone	Carb.	vein concentrate, post-dolomite
"	dolomite	2.2	− 12.87	− 6.06	24.61	sandstone	Carb.	vein concentrate
328vb	calcite	9.0	− 10.29	− 5.66	25.03	sandstone	Carb.	vein concentrate, post-dolomite
"	dolomite	5.6	− 11.12	− 5.53	25.16	sandstone	Carb.	vein concentrate
Footwall, damage zone								
322	calcite	1.3	− 20.22	− 8.57	22.03	sandstone	U. Carb.	vein
323	calcite	1.0	− 16.00	− 8.05	22.56	sandstone	U. Carb.	vein
Footwall, peripheral fracture zone outside main fault zone								
327	calcite	0.007	− 10.06	− 6.83	23.79	sandstone	U. Carb.	vein
3. Lower Camiri fault								
Hanging wall, damage zone								
333	calcite	3.9	− 15.84	− 13.15	17.30	sandstone	U. Carb.	matrix concentrate
333v	calcite	17.9	− 14.97	− 12.84	17.62	sandstone	U. Carb.	vein concentrate
332	calcite	1.5	− 15.75	− 13.55	16.89	sandstone	U. Carb.	matrix concentrate
332v	calcite	6.3	− 15.52	− 13.30	17.15	sandstone	U. Carb.	vein concentrate
Footwall, damage zone								
349	calcite	1.1	− 16.58	− 13.94	16.40	sandstone	U. Carb.	matrix
350	calcite	2.7	− 15.84	− 13.86	16.57	sandstone	U. Carb.	vein + matrix
Footwall, outside fault zone								
351	calcite	4.0	− 15.69	− 13.50	16.92	sandstone	U. Carb.	matrix
4. Cuevo fault								
Hanging wall, outside fault zone								
283	calcite	2.7	− 22.55	− 11.74	18.75	sandstone	U. Devonian	matrix
279	Mg-siderite	1.3	− 1.90	− 7.73	22.89	sandstone	U. Devonian	matrix
Hanging wall, damage zone								
277	calcite	0.4	− 6.19	− 11.45	19.06	sandstone	U. Devonian	vein, post-Mg-siderite
"	Mg-siderite	1.1	− 3.20	− 8.41	22.18	sandstone	U. Devonian	matrix
5. Carohuaicho fault								
Hanging wall, peripheral fracture zone outside main fault zone								
352	calcite	9.5	0.26	− 5.53	25.26	sandstone	U. Devonian	vein + matrix

(continued on next page)

Table 1 (*continued*)

Sample[a]	Carbonate	% Carb.[b]	δ13-C ‰ PDB	δ18-O ‰ PDB	δ18-O ‰ SMOW	Host-rock	Host-rock age	Remarks[c]
6. Tunal fault								
Hanging wall, outside fault zone								
73A	calcite	2.7	− 7.63	− 15.88	14.49	sandstone	Silurian	matrix
Footwall, fault core								
69	calcite	>75	− 3.06	− 16.06	14.30	shale	Devonian	vein
7. Piedra Larga fault								
Footwall, reverse fault system outside main fault zone								
203	calcite	2.9	− 10.17	− 8.65	21.66	sandstone	L. Permian	matrix
216	calcite	2.3	− 6.16	− 8.00	22.61	sandstone	L. Permian	vein + matrix
211	calcite	6.5	− 7.72	− 7.27	23.37	sandstone	L. Permian	vein + matrix
9. Honduras well fault								
Hanging wall, outside fault zone								
287	calcite	5.6	− 19.64	− 13.21	17.24	sandstone	L. Devonian	vein + matrix
Footwall, fault core								
288	magnesite	4.2	− 10.46	− 12.63	17.86	anhydrite/shale	L. Trias	sedimentary carbonate
289	magnesite	0.1	− 9.97	− 11.75	18.76	anhydrite/shale	L. Trias	sedimentary carbonate
Footwall, damage zone								
291	dolomite	18.4	− 5.64	− 6.76	23.89	silty dolomite	U. Permian	sedimentary carbonate
291v	dolomite	16.0	− 6.31	− 8.95	21.63	silty dolomite	U. Permian	vein concentrate
292	dolomite	25.0	− 7.02	− 4.73	25.98	silty dolomite	U. Permian	sedimentary carbonate
292v	dolomite	47.2	− 6.68	− 11.13	19.39	silty dolomite	U. Permian	vein concentrate
293	dolomite	2.2	− 7.53	− 8.31	22.32	silty dolomite	U. Permian	sedimentary carbonate
10. El Pajonal fault								
Hanging wall, outside fault zone								
248	calcite	6.4	− 8.40	− 13.31	17.14	sandstone	Tertiary	matrix
249	calcite	3.2	− 6.65	− 9.11	21.47	sandstone	Jurassic	matrix
250	calcite	trace	− 5.20	− 5.56	25.13	sandstone	Jurassic	matrix
251	calcite	0.2	− 11.10	− 9.31	21.27	sandstone	Trias	matrix
106	calcite	9.0	− 1.25	− 12.90	17.56	sandstone	Trias	matrix
253	calcite	0.1	− 4.80	− 7.55	23.08	sandstone	Trias	matrix
254	dolomite	8.9	− 0.64	1.73	32.67	sandstone	Trias	vein + matrix
Footwall, fault core								
150	calcite	0.3	− 7.86	− 8.65	21.94	sandstone	Tertiary	vein + matrix
154	calcite	0.6	− 7.68	− 7.31	23.32	sandstone	Tertiary	vein + matrix
255	calcite	1.3	− 7.64	− 10.17	20.38	sandstone	Tertiary	vein + matrix
104	calcite	0.2	− 10.09	− 7.99	22.62	sandstone	Tertiary	vein + matrix
	dolomite	0.2	− 7.39	− 10.53	19.16	sandstone	Tertiary	vein + matrix
155	calcite	0.6	− 7.35	− 10.47	20.07	sandstone	Tertiary	vein + matrix
156	calcite	0.4	− 7.85	− 9.09	21.49	sandstone	Tertiary	vein + matrix
157	calcite	0.1	− 7.00	− 8.76	21.83	sandstone	Tertiary	vein + matrix
158	calcite	0.4	− 7.78	− 9.11	21.47	sandstone	Tertiary	vein + matrix
103	calcite	1.6	− 8.09	− 9.02	21.56	sandstone	Tertiary	vein + matrix
160	calcite	1.3	− 8.01	− 8.86	21.73	sandstone	Tertiary	vein + matrix
165	calcite	1.5	− 8.21	− 9.65	20.91	sandstone	Tertiary	vein + matrix
162	calcite	1.8	− 7.98	− 10.29	20.25	sandstone	Tertiary	vein + matrix
Footwall, damage zone								
164	calcite	1.0	− 8.26	− 10.98	19.54	sandstone	Tertiary	matrix
Footwall, fold-reverse fault system outside main fault zone								
166	calcite	1.3	− 8.16	− 12.02	18.47	sandstone	Tertiary	matrix
170	calcite	1.0	− 9.09	− 13.06	17.40	sandstone	Tertiary	matrix

Table 1 (*continued*)

Sample[a]	Carbonate	% Carb.[b]	δ13-C ‰ PDB	δ18-O ‰ PDB	δ18-O ‰ SMOW	Host-rock	Host-rock age	Remarks[c]
171	calcite	0.7	−8.52	−9.93	20.62	sandstone	Tertiary	matrix
172	calcite	1.6	−7.47	−10.32	20.22	sandstone	Tertiary	matrix
109a	calcite	2.9	−8.27	−13.14	17.31	sandstone	Tertiary	matrix
109b	calcite	3.3	−7.78	−11.58	18.92	sandstone	Tertiary	matrix
179	calcite	2.1	−8.29	−13.24	17.21	sandstone	Tertiary	matrix
175	calcite	4.6	−8.41	−12.42	18.06	sandstone	Tertiary	matrix
176	calcite	2.7	−8.58	−12.66	17.81	sandstone	Tertiary	matrix
177	calcite	5.8	−8.46	−12.79	17.66	sandstone	Tertiary	matrix
102	calcite	5.3	−8.37	−13.82	16.61	sandstone	Tertiary	matrix
180	calcite	2.7	−8.45	−12.31	18.17	sandstone	Tertiary	matrix
182	calcite	3.4	−8.37	−12.35	18.13	sandstone	Tertiary	matrix
183	calcite	1.6	−7.00	−9.66	20.90	sandstone	Tertiary	matrix
185	calcite	1.3	−7.82	−10.44	20.10	sandstone	Tertiary	matrix
186	calcite	1.9	−8.36	−11.65	18.85	sandstone	Tertiary	matrix
187	calcite	2.5	−8.05	−11.11	19.41	sandstone	Tertiary	matrix
189	calcite	1.3	−8.27	−10.81	19.72	sandstone	Tertiary	matrix
Footwall, outside fault zone, undeformed Tertiary								
190	calcite	0.9	−8.09	−9.28	21.29	sandstone	Tertiary	matrix
191	calcite	1.9	−8.53	−10.80	19.73	sandstone	Tertiary	matrix
192	calcite	6.5	−8.19	−14.18	16.24	sandstone	Tertiary	matrix
193	calcite	0.5	−7.99	−11.37	19.14	sandstone	Tertiary	matrix
98	calcite	1.6	−8.00	−14.51	15.90	sandstone	Tertiary	matrix
Footwall, outside fault zone, folded pre-Tertiary								
97	calcite	3.0	−8.55	−11.52	18.98	sandstone	Jur.–Cret.	matrix
90c	calcite	17.6	−11.07	−8.09	22.52	concretion	U. Permian	sedimentary carbonate
90s	dolomite	>31	−11.28	−3.46	27.32	silty dolomite	U. Permian	sedimentary carbonate
89	calcite	14.2	−9.07	−11.13	19.39	sandstone	L. Permian	matrix
95	calcite	0.4	−9.07	−12.02	18.47	sandstone	U. Carb.	matrix
96	calcite	8.6	−7.05	−13.05	17.41	sandstone	U. Carb.	matrix
11. Palos Blancos fault								
Hanging wall, outside fault zone								
117	calcite	4.1	−10.68	−8.82	21.77	sandstone	L. Carb.	vein + matrix
12. Rio Pilcomayo fault								
Hanging wall, damage zone								
258	dolomite	1.7	−25.58	−6.21	24.46	sandstone	U. Devonian	vein + matrix
259	dolomite	1.0	−22.53	−6.35	24.31	sandstone	U. Devonian	vein + matrix
260	dolomite	4.1	−26.07	−6.06	24.61	sandstone	U. Devonian	vein + matrix
261	dolomite	10.8	−10.08	−4.59	26.13	sandstone	U. Devonian	vein + matrix
Footwall, fault core								
257	dolomite	18.2	−17.90	−7.16	23.48	sandstone	Tertiary	matrix concentrate
257v	dolomite	>18	−19.59	−8.44	22.16	sandstone	Tertiary	vein concentrate
13. Aguaragüe fault								
Hanging wall, fault core								
119	calcite	1.8	−14.41	−10.75	19.78	sandstone	L. Carb.	vein + matrix
120	calcite	0.3	−8.71	−7.98	22.63	sandstone	L. Carb.	matrix

(continued on next page)

Table 1 (*continued*)

Sample[a]	Carbonate	% Carb.[b]	δ13-C ‰ PDB	δ18-O ‰ PDB	δ18-O ‰ SMOW	Host-rock	Host-rock age	Remarks[c]
13. Aguaragüe anticline hinge zone								
126	calcite	1.1	−23.65	−8.08	22.53	sandstone	M. Devonian	vein + matrix, post-Mg-siderite
	Mg-siderite	2.2	−22.78	−8.56	21.73	sandstone	M. Devonian	matrix
127	Mg-siderite	0.8	−12.16	−7.96	22.65	sandstone	M. Devonian	matrix
131	Mg-siderite	1.2	1.71	−7.69	22.93	sandstone	M. Devonian	matrix

[a] (") indicates dolomite or Mg-siderite chemically separated from calcite in the same sample as that on the line above.

[b] Yield data are only indicative.

[c] Vein: cement in fracture or cataclastic slip band; Matrix: intergranular cement in host-sandstone.

deformed crystals. This suggests that calcite precipitated in several stages before and during/after CSB formation, with the first generations being deformed inside the CSBs and the younger ones being precipitated only in the host-sandstone. The $\delta^{18}O$ values show a narrow range in both the footwall (16.3–18.6‰) and the hanging wall (14.8–17.4‰) (Table 1 and Fig. 11). On the other hand, there is a marked contrast in $\delta^{13}C$ values between the footwall (−9.6‰ to −11.9‰) and the hanging wall (−2.9‰ to −5.6‰).

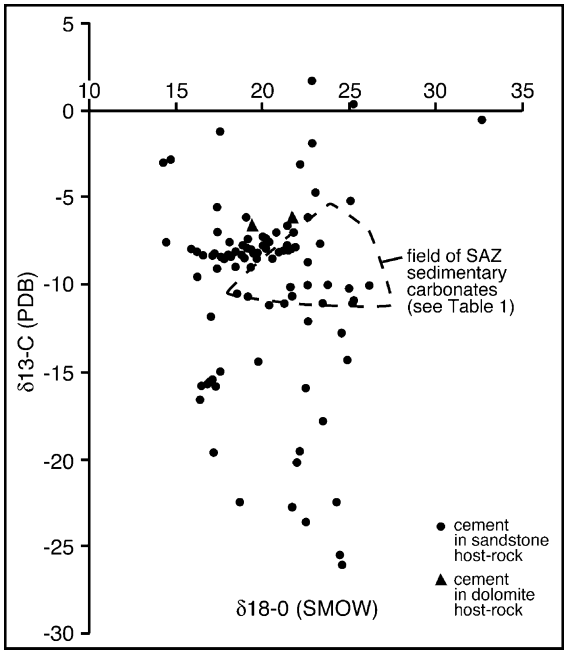

Fig. 10. Diagram of oxygen and carbon isotope ratios in carbonate cements showing all the samples analysed in this study (95 samples). Numerical values and sample data (sampling location, mineralogy, type of cement (matrix or fracture), nature and age of host-rock) are summarised in Table 1. The domain of sedimentary carbonates corresponds to seven samples of Upper Permian and Lower Triassic evaporites from Honduras and Pajonal faults footwalls summarised in Table 1. See Figs. 11 and 12 for detailed isotopic, mineralogic and structural relationships in selected fault zones.

7.4.2. Upper Camiri fault (2 in Fig. 1)

The fault places Upper Devonian low-porosity sandstones with a shale-rich, dm-thick basal detachment horizon above Upper Carboniferous high-porosity sandstones. In the main fault zone, calcite cement occurs only in veins in the footwall part (Figs. 3, 4 and 9J). This occurrence is remarkable because there is almost no matrix cement in the host-sandstone, in spite of its high porosity (Fig. 9J). Carbonate cement is absent in the external zones, but it is present in satellite fracture zones located a few tens of metres from the main fault zone in Carboniferous sandstones both in the footwall and hanging wall. The footwall fracture zone contains very minor calcite in CSBs. In the hanging wall, a first generation of dolomite was followed by a second generation of calcite in both extension veins and the host-sandstone (Fig. 9I). The range of isotopic values is similar in both fault compartments, with a small dispersion of the $\delta^{18}O$ values (22.0–23.8‰ in the footwall and 23.5–25.3‰ in the hanging wall) and large variations of $\delta^{13}C$ values, particularly in the footwall (−10.1‰ to −20.2‰ in the footwall and −10.3‰ to −14.4‰ in the hanging wall) (Table 1 and Fig. 11). In the hanging wall, the $\delta^{13}C$ value of calcite is always slightly higher than that of the associated dolomite.

7.4.3. Lower Camiri fault (3 in Fig. 1)

The fault places (Lower?) Carboniferous alternating low-porosity sandstones and shales above Upper Car-

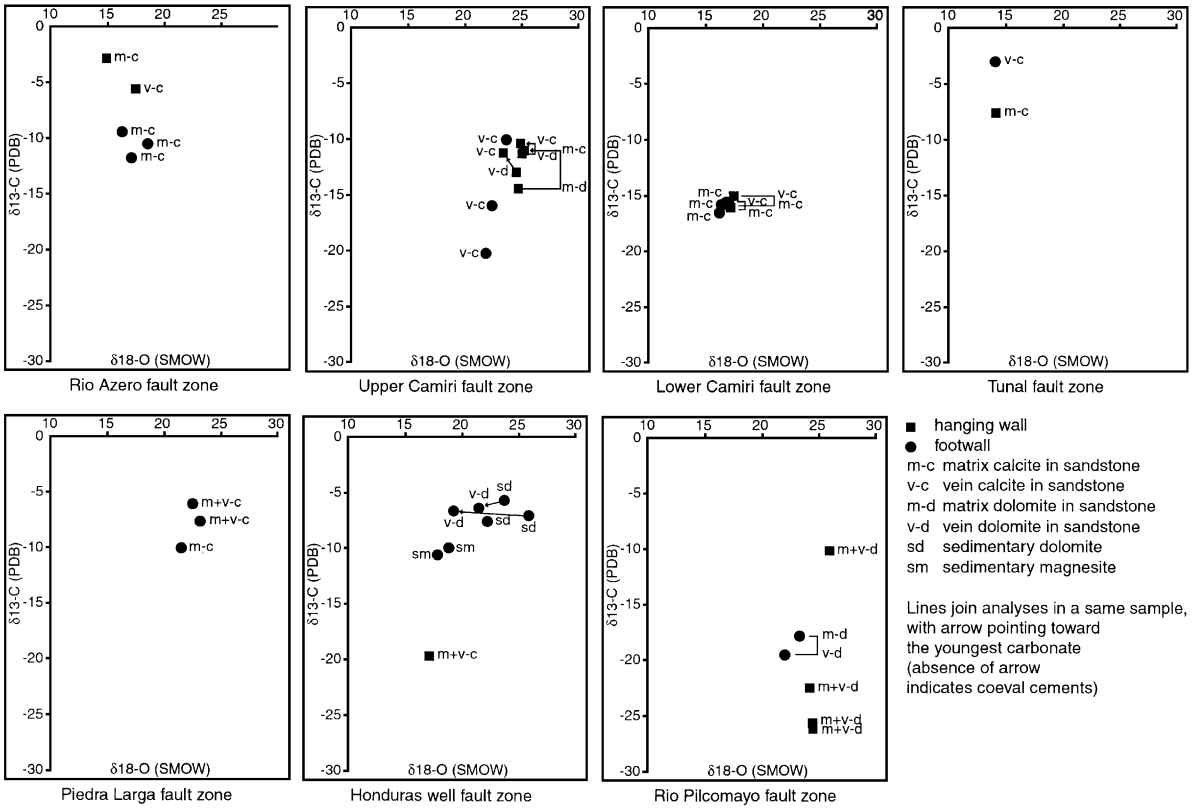

Fig. 11. Diagrams of oxygen and carbon isotope ratios in carbonate cements from selected fault zones. The structural location of cements in each fault zone is shown in Fig. 4. The samples of Piedra Larga and Upper Camiri faults are localised in Fig. 3.

boniferous sandstones with a higher porosity, the fault core being constituted by sheared claystone. Calcite cement is mostly restricted to the damage zones (Fig. 4). In the hanging wall, calcite occurs in shear and extension veins and host-sandstone with decreasing abundance upwards, but the outside of the fault zone cannot be observed. Some of the shear fractures show fibrous calcite-fill, attesting syn-faulting precipitation. The calcite-filled fractures post-date quartz-sealed CSBs. In the footwall, calcite is scarce in CSBs and host-sandstone and a little matrix calcite is also present in the few metres immediately below the fault zone. One calcite-cemented CSB is cut by a younger cm-long gypsum vein. In all samples, most calcite, both in veins/CSBs and host-sandstone, is bright orange luminescent, with a minor non-luminescent second generation in the hanging wall (Fig. 9E and F). All isotopic values of the hanging wall and footwall samples are very similar for both oxygen and carbon ($\delta^{18}O$ between 16.4‰ and 17.6‰; $\delta^{13}C$ between -15.0‰ and -16.6‰) (Table 1 and Fig. 11). In the hanging wall, these values include matrix and vein concentrates that could be analysed separately.

7.4.4. Cuevo fault (4 in Fig. 1)

The fault places Upper Devonian low-porosity sandstones above Tertiary high-porosity sandstones. Only the hanging wall part of the damage zone and adjacent external zone are exposed at outcrop, whereas the footwall is visible only several hundreds of metres east of the fault. In the hanging wall, carbonate cement was observed in only three of a total of 12 samples. In the damage zone, one sample contains Mg-siderite in the matrix and younger calcite in veins and matrix. Outside the fault zone, matrix cements are Mg-siderite + calcite in one sample and

calcite in another sample. The two Mg-siderite samples have roughly similar isotopic values for both oxygen (22.9‰ and 22.2‰) and carbon (− 1.9‰ and − 3.2‰) (Table 1). Two calcite samples have similar $\delta^{18}O$ values (19.6‰ and 18.7‰) but highly different $\delta^{13}C$ values (− 6.2‰ and − 22.5‰). No carbonate was observed in the footwall.

7.4.5. Carohuaicho fault (5 in Fig. 1)

The fault zone and footwall are not visible, but Upper Devonian sandstones outcrop about 100 m above the fault, with a m-scale fold in the lower part considered as satellite deformation of the major fault. Calcite cement occurs in CSBs and host-sandstone in the fold and is absent in the overlying undeformed beds ($\delta^{18}O = 25.1‰$; $\delta^{13}C = 0.3‰$) (Table 1).

7.4.6. Tunal fault (6 in Fig. 1)

The fault places Silurian above Devonian rocks, both consisting of alternating low-porosity sandstones and shales (the latter more abundant in the footwall). In the fault zone, calcite cement is present in shear and extension veins and host-sandstone in the footwall part and in the matrix in the hanging wall part (Fig. 4). The shear fractures show fibrous calcite-fill in dilational jogs, attesting syn-faulting precipitation. Outside the fault zone, one thin extension calcite vein with a crack-seal structure was observed in the hanging wall. The outside part of the fault zone cannot be observed in the footwall. The $\delta^{18}O$ values are very similar on both sides of the fault (14.5‰ in the hanging wall and 14.3‰ in the footwall), but the $\delta^{13}C$ values are quite different (− 7.6‰ in the hanging wall and − 3.1‰ in the footwall) (Table 1 and Fig. 11).

7.4.7. Piedra larga fault (7 in Figs. 1 and 2)

The fault zone places Lower Devonian low-porosity sandstones with a few metres thick shale-rich basal detachment horizon above Upper Carboniferous low-porosity sandstones and diamictites, themselves overlying higher porosity Lower Permian sandstones. The latter are affected by a reverse fault system localised about 200 m below the main fault. There is no carbonate cement in the main fault zone and adjacent external zones, except very little calcite in one sample from the hanging wall fault core. In contrast, calcite cement occurs in CSBs, shear veins and host-sandstone in the faulted Lower Permian sandstones, with a higher abundance in the most fractured samples (Figs. 3 and 4). The calcite-filled structures post-date quartz-sealed CSBs. Some shear veins feature calcite-filled dilational jogs, one of them with a crack-seal structure, attesting syn-faulting precipitation. Calcite is red-luminescent, with zoning marked by variations of CL intensity in the thickest veins. Variations of $\delta^{18}O$ values are limited (21.7–23.4‰), but variations of $\delta^{13}C$ values are larger (− 6.2‰ to − 10.2‰) (Table 1 and Fig. 11).

7.4.8. Honduras well fault (9 in Figs. 1 and 2)

The fault places Lower Devonian low-porosity sandstones above intensely sheared Lower Triassic shale and anhydrite forming the fault core and Upper Permian fractured silty dolomite forming the damage zone (Fig. 4). The hanging wall was cored about 200 m above the fault, where it features calcite cement in veins and host-sandstone post-dating quartz-sealed cataclasite. The hanging wall part of the fault zone was not cored and it is only known by cm-sized tectonic lenses of cataclastic sandstone included by tectonic mixing in the footwall part of the fault core. In the latter, anhydrite reworked by dissolution–precipitation fills numerous extension and shear fractures across, and pressure shadows around, competent sandstone and anhydrite lenses. In contrast, the evaporites also contain magnesite that was not reworked during faulting. Vein and matrix calcite cement occurs only in the sandstone lenses where it post-dates quartz-sealed cataclasite and it is post-dated itself by the anhydrite veins, which suggests that calcite precipitation occurred in the hanging wall, before the sandstones were tectonically included in the footwall. In the footwall damage zone, the silty dolomite is affected by numerous shear and extension fractures. Most of these fractures are filled by dolomite, locally with a crack-seal structure, and many of them also contain post-dolomite anhydrite cement. CL observation shows two generations of vein dolomite (dull greenish then brownish luminescent), different from the yellow-luminescent host-dolomite. In the hanging wall external zone, the isotopic values of calcite are of 17.2‰ for oxygen and − 19.4‰ for carbon (Table 1 and Fig. 11). In the footwall fault core, the values of evaporitic magnesite are of 17.9‰ to 18.8‰ for oxygen and − 10‰ to − 10.5‰ for carbon. In the damage zone, the $\delta^{13}C$ values are similar for the vein

dolomite (− 6.3‰ to − 6.7‰) and the host sedimentary dolomite (− 5.6‰ to − 7.5‰), but the $\delta^{18}O$ values are slightly lower for the veins (19.4–21.6‰) than for the host (22.3–26.0‰).

7.4.9. Pajonal fault (10 in Figs. 1 and 2)

The fault places Mesozoic porous sandstones with a basal detachment horizon in Lower Triassic shales and gypsum above high-porosity Tertiary sandstones. In the main fault zone, calcite cement occurs only in the footwall, in CSBs, shear and extension veins and host-sandstone (Fig. 4). Calcite in dilational jogs indicates syn-faulting precipitation. The calcite-filled structures post-date quartz-sealed cataclasite. By contrast, the hanging wall shales and gypsum contain only gypsum veins A few gypsum veins also occur in the uppermost part of the footwall cataclasite, some of them cutting the fault surface and being physically connected with the sedimentary gypsum layer at the base of the hanging wall.

Below the main fault zone, the upper part of the Tertiary succession is affected by a 100-m thick fold-reverse fault system where calcite cement is relatively common in the sandstone matrix. This system is also remarkable by the occurrence of numerous, up to several metres long, extensional gypsum veins with both low and steep dips, the latter indicating E–W to NE–SW extension (i.e., sub-parallel to the local compressional structures). These veins always occur across or close to (i.e., up to a few metres from) conglomerate layers that bear gypsum pebbles (probably derived from the Lower Triassic of the hanging wall by syntectonic sedimentation during thrust emplacement). Gypsum cement is also present in the host-sandstone of the veins. The cross-cutting relationships show that gypsum veins post-date both the fold-reverse fault deformation and the calcite cement.

Outside the fault zone, we sampled sandstones along a 20-km-long section comprising the whole hanging wall Mesozoic succession and the whole footwall Tertiary succession and its Mesozoic–Palaeozoic substratum down to the Upper Carboniferous (Fig. 2). All these sandstones feature a medium to high porosity. Many samples contain a trace to a few percent (<5%) of calcite matrix cement, although some contain none. One sample from the hanging wall Triassic contains dolomite cement in fracture and host-sandstone.

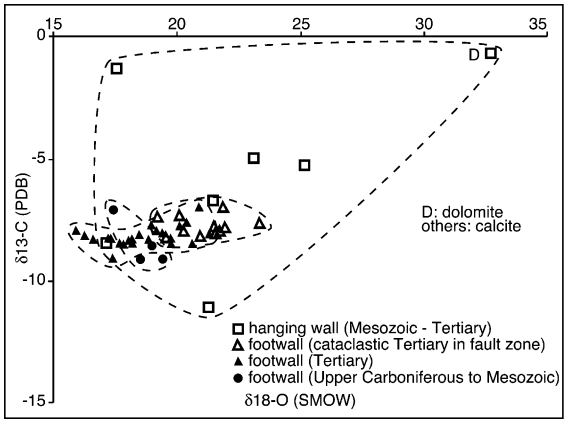

Fig. 12. Diagram of oxygen and carbon isotope ratios in carbonate cements in the Pajonal fault zone and hanging wall and footwall sections (the sampled cross-section, about 20 km long, is localised in Fig. 2; the structural location of cements around the Pajonal fault zone is shown in Fig. 4).

In the footwall, the $\delta^{13}C$ values outside the fault zone are uniform (<± 1‰) both in the Tertiary (− 7.0‰ to − 9.1‰) and the underlying Mesozoic–Palaeozoic (− 7.1‰ to − 9.1‰) (Table 1 and Fig. 12). The $\delta^{18}O$ values are also similar in both intervals, but with higher dispersion in the Tertiary (15.9–21.3‰) than in the Mesozoic–Palaeozoic (17.4–19.4‰). In the lower part of the fault zone, the $\delta^{18}O$ values are similar to those immediately below the fault zone, but they increase progressively to higher values when approaching the fault contact (from 19.5‰ to 23.3‰), whereas the carbon values remain similar to those below the fault zone (− 7.0‰ to − 8.3‰). In the hanging wall, the carbonates show a very large dispersion of isotopic values ($\delta^{18}O$ between 17.2‰ and 32.7‰, and $\delta^{13}C$ between − 11.1‰ and − 0.6‰), with the highest values of both oxygen and carbon in the dolomite sample.

7.4.10. Palos Blancos fault (11 in Fig. 1)

The fault zone and footwall are not visible, but Lower Carboniferous sandstones, diamictites and shales outcrop about 100 m above the fault. One sample contains calcite cement in veins and host-sandstone ($\delta^{18}O = 21.8‰$; $\delta^{13}C = -10.7‰$) (Table 1).

7.4.11. Rio Pilcomayo fault (12 in Figs. 1 and 2)

The fault places Upper Devonian low-porosity sandstones above Tertiary high-porosity sandstones.

Dolomite cement is present in the hanging wall damage zone and footwall fault core (Fig. 4). There is no carbonate in the hanging wall external zone, but the footwall damage and external zones are not visible. In the footwall, dolomite is abundant in CSBs and host-sandstone. Some of the CSBs feature late dilational jogs indicating syn-faulting precipitation (Fig. 9A and B). In the hanging wall, dolomite is mainly present in extension and shear fractures, but it is scarce in the host-sandstone where it precipitated as isolated crystals in secondary pores resulting from feldspar grain dissolution (Fig. 9G and H). In both compartments, dolomite in both veins/CSBs and host-sandstone is often zoned and composed of a bright yellow luminescent first generation and an orange luminescent second generation, each one with fine zoning marked by variations of CL intensity (Fig. 9B and H). A dull-luminescent, also zoned, third generation is present both in the CSBs and host-sandstone of the footwall (Fig. 9B). The $\delta^{18}O$ values are rather similar in both compartments, although they are slightly lower in the footwall (22.2–23.5‰) than in the hanging wall (24.3–26.1‰) (Table 1 and Fig. 11). By contrast, the $\delta^{13}C$ values are highly variable (-10.1‰ to -25.6‰), the two extreme values being in the hanging wall. In the hanging wall, the analyses were made on whole rocks. In the footwall, CSB and matrix concentrates were analysed separately and gave similar values.

7.4.12. Aguarague fault and anticline hinge zone (13 in Figs. 1 and 2)

The fault places Lower Carboniferous low-porosity sandstones above Upper Carboniferous high-porosity sandstones (Fig. 4). Only the hanging wall part of the fault zone is visible, with little calcite cement in veins and host-sandstone, and the footwall outcrop begins about 20 m below the fault, without cement in the uppermost part. However, different cements have been locally observed in the footwall. About 200 m below the fault, calcite and gypsum form mm-across isolated patches of matrix cement in the Upper Carboniferous sandstones. In the anticline hinge zone, about 3 km east of the fault, Mg-siderite matrix cement occurs in Middle–Upper Devonian low-porosity sandstones alternating with shale layers and affected by fractures and m-scale folds related to the large fold. Two samples also contain a cement posterior to the Mg-siderite, one of calcite in CSBs and host-sandstone and another of gypsum in a small extension vein. Most $\delta^{18}O$ values are very similar for all outcrops and all carbonates (21.7–22.9‰ for the Mg-siderite and 19.8–22.6‰ for calcite). By contrast, the $\delta^{13}C$ values are highly variable for each outcrop and each carbonate (1.7‰ to -22.8‰ for the Mg-siderite, -8.7‰ and -14.4‰ for the fault zone calcite and -23.6‰ for the anticline hinge zone calcite) (Table 1).

8. Origin of carbonate cements and carbonate-precipitating fluids

In the essential absence of sedimentary carbonates in the SAZ sandstones, the widespread presence of carbonate cements implies their introduction from outside sources via a fluid. Internal sources of calcium are estimated to contribute less than a tenth of a percent of carbonate, assuming that the 10–20% of alkali feldspar typically contains $\sim$0.4 wt.% CaO (Deer et al., 1963). Ca-feldspars are absent and the contribution of calcium from the minor clays and very rare apatite is trivial. The Upper Permian sedimentary (evaporitic) carbonates and the Paleogene paleosoils may have provided part of the calcium, but these formations are only a few metres to tens of metres thick and thus seem too localised sources for carbonates distributed throughout the whole thrust system. Alternatively, dissolution of fossils in the shale layers is a more likely source of calcium. Mg-siderite (Cuevo, Aguarague) and most of the dolomites (upper Camiri, Rio Pilcomayo) occur within or near alternating shales-sandstones, implying the role of the local shales as a source of Fe and Mg. Importation of carbonate cations in sandstones may have occurred by diffusion from neighbouring shales in the cases of alternating dm-thick sandstone and shale layers. However, transport of dissolved carbonate by diffusion is restricted to limited distances (Renard et al., 2000) and transport by fluid flow is a more likely origin for carbonate cementation in most sandstone formations.

The markedly ^{13}C-depleted nature of the majority of carbonate cements in sandstones from all outcrops and stratigraphic formations (Table 1 and Fig. 10) suggests that the source of the carbonate carbon must be principally related to the evolution of organic

complexes, and not just to the remobilisation of normal marine sedimentary carbonates whose $\delta^{13}C$ values are $> -1‰$. Although a contribution of mantle-derived carbon dioxide with $\delta^{13}C \sim -5‰$ (e.g., Ballentine and O'Nions, 1994) cannot be discounted, it is probably negligible in a non-extensional crustal environment. Therefore, carbonate precipitation should have been contemporaneous with the leakage of CO_2/CH_4 from the hydrocarbon source rocks, mainly the Silurian and Devonian shales. The location of the most ^{13}C-depleted values may reflect their proximity to the hydrocarbon source and/or reservoir formations, i.e. the Devonian shales and Carboniferous sandstones, respectively.

The source of the carbonate oxygen is related to the aqueous fluids which circulated through the rocks. The wide range of $^{18}O/^{16}O$ ratios of the carbonates requires that precipitation took place over both a range of temperatures and $\delta^{18}O$-water values. Based on the observation that the carbonate cements contain a vast majority of very small and monophase aqueous fluid inclusions, temperatures of carbonate precipitation are inferred to have been $< \sim 80$ °C (Goldstein and Reynold, 1994).

The $^{18}O/^{16}O$ ratios of waters in equilibrium with carbonate can be calculated from the experimental carbonate–water fractionation data (O'Neil et al., 1969 for calcite and combining the data of O'Neil et al., 1969; Sheppard and Schwarcz, 1970; Matthews and Katz, 1977 for dolomite) and the temperature. The calculated values are summarised in Fig. 13 for temperatures < 100 °C. Because the great majority of calcites have $\delta^{18}O$ values between 14.3‰ and 26‰, two curves for water in equilibrium with such calcites define a band of water values as a function of temperature in Fig. 13. Also included are a range for estimated values of Tertiary and younger sea waters and data for two rivers near Potosi (Grant et al., 1980), about 250 km NW of our region. For our SAZ area at an altitude of ~ 2000 m, Recent to Tertiary meteoric $\delta^{18}O$ values are estimated to have been in the $-6‰$ to $-9‰$ range, based on a $\sim -2‰$/km altitude effect because of the difference in altitude relative to Potosi (~ 4000 m) and the general increase in altitude of the area since the Tertiary due to the uplift of the Andes.

From inspection of Fig. 13 and application of the above constraints, the following generalisations can be made about the aqueous fluids.

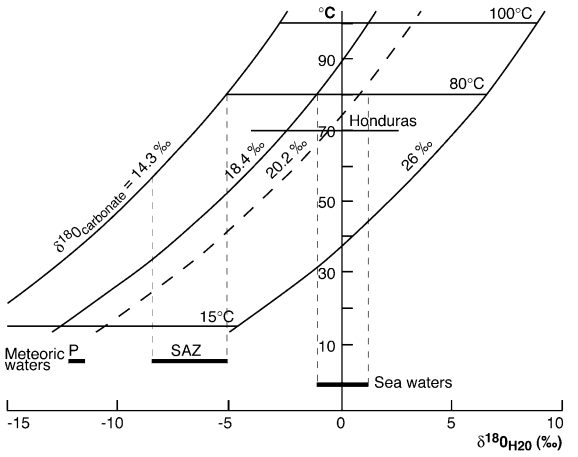

Fig. 13. Temperature vs. $\delta^{18}O$-water. Ranges of $\delta^{18}O$-water values are shown for Tertiary to Recent sea waters, two rivers near Potosi and estimated values for Recent to Tertiary meteoric waters in the SAZ. Curves are given for water in equilibrium with the extreme values of calcite at 14.3‰ and 26‰, mean calcite at 20.2‰ and calcite at 18.4‰ (see text for discussion). The range of $\delta^{18}O$ values for the Honduras well samples is shown at the present temperature of about 70 °C (estimated from the sampling depth and present geothermal gradient (see text)).

(1) For all carbonates with $\delta^{18}O < 18.4‰$, a meteoric water contribution is necessary, with precipitation temperatures between 35 and 80 °C. This concerns 28 samples from various domains both inside and outside fault zones and in various stratigraphic formations (Upper Devonian and Tertiary at Rio Azero, Upper Carboniferous at Lower Camiri, Silurian and Devonian at Tunal, Lower Devonian at Honduras, Triassic in Pajonal hanging wall, Upper Carboniferous and Tertiary in Pajonal footwall).

(2) For all carbonates with $\delta^{18}O > 18.4‰$ (67 samples from all fault zones, except Rio Azero, Lower Camiri and Tunal, and all stratigraphic formations except Silurian), sea water (connate waters) could have been a dominant, but not essential, constituent.

(3) For average fault zone carbonate with $\delta^{18}O = 20.2‰$, temperatures of precipitation were >20 °C and, if < 65 °C, a meteoric water contribution is essential.

(4) The most ^{18}O-depleted calcites at $\sim 15‰$ (from Tunal and Rio Azero) require precipitation temperatures >50 °C from isotopically unmodified meteoric waters.

(5) If meteoric waters were a major source of all formation waters, then many of the meteoric waters must have either undergone enrichment in ^{18}O, through exchange reactions with minerals, or mixed with more ^{18}O-rich waters (sea water and/or deep formation water). For formation waters with $\delta^{18}O > +1.2‰$, implying precipitation temperatures >50 °C for these samples, waters more enriched in ^{18}O than unmodified sea waters are required. Based on observations from many other sedimentary basins, temperatures of mineral-water exchange were probably $> \sim 75$ °C (see Fig. 5 in Sheppard, 1986).

(6) Of the 12 fault systems with marine rocks, half (Rio Azero, Lower Camiri, Cuevo, Tunal, Honduras, Pajonal) have cements, in marine host-rock, whose $\delta^{18}O$-water values were $< 0‰$, implying that they contained a more or less important meteoric water component.

In summary, at least $\sim 30\%$ of both inside and outside fault zone carbonates require a significant meteoric water contribution in the precipitating fluids. These same carbonates also need precipitation temperatures >35 °C and certain >50 °C. Although the great majority of the carbonates could have been precipitated from aqueous fluids of dominantly meteoric origin, requiring temperatures of 15–80 °C with temperature increasing with decrease in $\delta^{18}O$-calcite, a mixed meteoric-sea water or modified meteoric water (e.g., deep hot formation water) origin provides a more reasonable explanation for many of the more ^{18}O-rich carbonates ($> \sim 20‰$), particularly if precipitation temperatures were >40 °C. Carbonate-precipitating fluids in pre-Tertiary rocks, most of which had a relatively high temperature burial history (maximum of 120–200 °C), have $\delta^{18}O$-water values comparable to those that have only experienced a relatively near surface history ($< \sim 3$ km depth or < 80 °C).

9. Carbonate-precipitating fluid flow in fault zones and thrust sheets

The preferential concentration of carbonate in most of the studied fault zones, compared to the adjacent external zones, suggests that they acted as preferential pathways for longitudinal carbonate-precipitating fluid flow. Below, we first discuss the structure of small-scale permeability in fault zones. Then, combining structural, carbonate paragenesis and isotope data, we show that the different fault zones had different hydraulic behaviours at the outcrop scale that can be grouped in 3 main types. This typology is discussed based on the study of the 8 faults where both fault zone compartments could be observed. Finally, we discuss the relationships between fluid flow in fault zones and adjacent thrust sheets.

9.1. Structure of small-scale permeability in fractured sandstones

The origin of high permeability of sandstones in the non-quartz-sealed fault zones probably results from the high density of connected fractures. Preferential fluid circulation in fractures is well illustrated by those carbonate-cemented transgranular fractures whose host-sandstone contains no or very little carbonate cement in spite of a relatively high matrix porosity (Fig. 9I). Therefore, we infer that, in the case of the low-medium porosity sandstones, the transgranular fractures were the preferential drains through which the fluid circulated in fault zones and then percolated in the host-sandstones (Fig. 9E–H).

In contrast, a sealing effect would be expected for CSBs in porous sandstones, because the low porosity of uncemented CSBs (Fig. 7A and B) is known to imply a very low permeability compared to that of the porous host-sandstone (Antonellini and Aydin, 1994; Fowles and Burley, 1994). This effect is observed at Rio Azero where the footwall CSBs contain little and intensely deformed calcite, whereas the host-sandstone contains abundant, younger matrix calcite cement. However, the frequent observation that carbonate precipitation in CSBs implied strong dilation of the grain fragments, shows that these structures could be permeable to fluid flow (Fig. 10A and B). This agrees with the observation by Evans et al. (1998) of dolomite-cemented CSBs that acted as preferential pathways for fluid flow. This behaviour is probably due to the very high density of connected fractures which give to the CSBs a high dilation potential in the case of favourable mechanical conditions, in spite of their very low porosity. These conditions could be related to the CSB kinematics (i.e., domains corresponding to dilational jog during shear movement (Fig. 9C) or late extensional reactivation) and/or transient episodes of high fluid pressure. The abundance of carbonate

cement in CSBs may also be favoured by easy nucleation due to the high surface/volume ratio, with most of the surfaces being clean fractures. The development of intragranular fractures and grain rotations outside the CSBs are likely to be important due to their low cohesion; they may also have contributed to enhance fault zone permeability compared to the original sandstone, as observed at the periphery of certain CSBs by Fowles and Burley (1994). Hence, the high permeability of fault zones in porous sandstones would not only be related to the CSBs, but it may also be a bulk characteristic of host-sandstones.

9.2. Typology of carbonate-precipitating fluid flow in fault zones

9.2.1. Common fluids for both fault zone compartments

At Lower Camiri, the fact that all cements are calcite with similar CL characteristics and isotopic values strongly suggests that carbonates in both compartments and in both veins/CSBs and host-sandstone precipitated from similar fluids (excepting the minor late generation in the hanging wall). This conclusion seems to be contradictory with the occurrence of a several m-thick claystone horizon in the fault core, which should have formed a seal between the two damage zones. We suggest that this seal has probably a poor lateral continuity, the two damage zones being hydrologically connected for lateral fluid flow where the seal pinches out. On the other hand, the disappearance of calcite cement going away from the fault shows the lack of transversal fluid flow.

At Rio Pilcomayo, dolomite is common to both fault compartments, but the zoning of dolomite crystals suggests circulation of several fluid pulses. CL observation indicates that these pulses belonged to three main fluid generations, the first two being common to both compartments and the third one being restricted to the footwall. The similar oxygen isotope ratios argue for fluid pulses having a common origin and temperature with little or no mixing, but the carbonate, with highly variable $\delta^{13}C$ values, was derived from either a single but evolving hydrocarbon source or different ones. Because the several CL generations of dolomite could not be analysed separately, we do not know if each fluid generation comprised packets of fluids with different $^{13}C/^{12}C$ ratios that circulated in different parts of the fault zone, or if each generation corresponded to a fluid packet isotopically homogeneous at the scale of the fault zone, with the different samples analysed reflecting the mixing of the different generations in variable proportions. The abundance of dolomite both in CSBs and host-sandstone as well as the presence of the most complete CL stratigraphy in the footwall suggests that most of the fluid flow was located there due to the high porosity of the Tertiary sandstones, whereas circulation in the hanging wall was more limited (only two main CL generations) and mostly restricted to fractures in the less porous Upper Devonian sandstones.

The similar history of carbonate-precipitating fluid flow for both compartments of these fault zones has two important implications. First, inside the fault zone, the fault contact was not a barrier to transversal flow. Second, although carbonate precipitation in dilational jogs attests to syn-thrust faulting fluid flow, it implies that flow occurred during the late stages of fault activity, i.e. when the present stratigraphic juxtaposition was (close to being) achieved and both compartments were submitted to similar fluids (fluid–rock interaction history) at like temperatures.

9.2.2. Different fluids for each fault zone compartment

At Rio Azero and Tunal, calcite occurs in both fault zone compartments, but with different isotopic characteristics. Specifically, in each fault zone the two compartments show rather similar oxygen values but carbon values different from each other, indicating fluids derived from different sources. At Rio Azero, the carbon values also show variations in each compartment, again interpreted in terms of pulsating fluids. Microstructural data attest syn-thrust-faulting fluid flow, at least in the footwall compartment of each fault zone (calcite in dilational jogs at Tunal; alternating calcite precipitation and CSB formation at Rio Azero). The latter observation is also another indication of pulsated fluid flow.

The fact that the two compartments of these fault zones saw carbonate-precipitating fluids with different histories from each other indicates that either the contact was a barrier to transverse flow for the different fluid pulses, or the carbonates precipitated during an early stage of thrust activity (or at different stages), i.e. when the currently adjacent compartments were

still separated in distance and burial depth, and fluid conditions were thus different in the separate compartments.

9.2.3. No fluid flow in one or both main fault zone compartment(s)

At Upper Camiri, carbonate-precipitating fluid flow in the main fault zone occurred only in the footwall sandstones, whereas no carbonate was found in the shaly basal detachment and low-porosity sandstones in the hanging wall. Moreover, fluid flow was restricted to fractures in spite of the rather high porosity of the host-sandstone. Fluid flow also occurred in the satellite fracture zones located in the footwall and hanging wall, a few tens of metres away from the main fault zone. In the footwall, the similar oxygen isotope values and highly variable carbon values are again interpreted in terms of pulsating fluids, with each pulse with its own pathway. By contrast, the change of mineralogy and the variable isotopic values (mainly for carbon) in a same hand specimen from the hanging wall attest to several pulses circulating in the same fracture system. The similar isotopic values between certain calcites from the footwall and hanging wall satellite fracture zones suggest a possible hydrologic connection of these zones, implying that calcite precipitated late during/after thrust-faulting.

At Piedra Larga, there is no carbonate in the low porosity rocks involved in the main fault zone (shales and sandstones in the hanging wall, diamictites and sandstones in the footwall), except minor calcite cement in one sample from the hanging wall fault core, and carbonate-precipitating fluid flow was restricted to the more porous footwall Permian sandstones. In the latter, the fact that (i) most of the carbonate is concentrated in fractures of the reverse fault system and (ii) some shear veins contain calcite in dilational jogs, locally with a crack-seal structure, well illustrates the structural control of fluid flow during thrust-faulting. The similar isotope values for oxygen and different values for carbon and CL zoning of calcite in some veins indicate various pulses of fluids.

At Honduras, calcite-precipitating fluid flow was restricted to the Lower Devonian sandstones of the hanging wall (fault zone cataclasite and fracture in external zone). By contrast, cements in the footwall were most probably derived from local rocks and do not necessarily imply fluid circulation (anhydrite cement in the fault core and dolomite cement in the damage zone), or they imply a fluid allochthony limited to a few metres (the anhydrite cement in the damage zone). This interpretation is confirmed by the isotopic values of dolomite which show that the vein carbon is probably derived from the host sedimentary dolomite through dissolution/precipitation, but the oxygen isotope differences require fluids with different $\delta^{18}O$ values (i.e., different mixing or fluid–rock interaction histories) and/or higher temperatures for vein formation.

In these faults, the fact that one or both compartments of the main fault zone did not see fluid flow can be ascribed to the low porosity (permeability) of rocks (shales, compacted sandstones, anhydrite, dolomite) forming these compartments, which constrained fluid flow in the more porous adjacent rocks. A similar situation occurred at Pajonal (see below). At Honduras, this effect may have been enhanced by rapid sealing of footwall fractures by local minerals, that prevented percolation of the fluids that circulated in the hanging wall.

9.3. Fluid flow in the Pajonal fault zone and adjacent thrust sheets

From the very extensive sampling across the hanging wall and footwall sandstone formations at Pajonal, the nature of fluid flow within the fault zone can be compared with that in the kilometre-thick adjacent thrust sheets. In the main fault zone, carbonate-precipitating fluid flow was restricted to the footwall Tertiary sandstone cataclasite, whereas the low-porosity Triassic shales and gypsum forming the hanging wall part contain only gypsum veins. On the studied section, evidence of carbonate-precipitating fluid flow is also frequent in porous sandstones of adjacent thrust sheets.

The similarity of the $\delta^{13}C$-calcite values in the footwall succession, including the main fault zone and the fold-reverse fault system, strongly supports a common origin. Precipitation temperatures would also have to be very similar. Because the carbonate had to be imported from outside of the immediate system, a common aqueous fluid for its transportation is implied. The more variable $\delta^{18}O$ values are not

necessarily in contradiction with this interpretation, because fluid mixing must have occurred with the carbon-poor formation waters initially present in the relatively porous and permeable sandstones outside the fault. Small variations in the mixing ratio would influence the δ^{18}O-calcite values but not their δ^{13}C values. On a metric scale, the progressive increase of δ^{18}O-calcite across the footwall part of the fault zone on approaching the fault surface indicates that when the fault zone cataclasite changed from quartz-sealed to non-quartz-sealed, it became a drain for a fluid slightly different, but related, to that circulating outside the fault. This is consistent with fluid mixing between fault zone and external zone fluids. Alternatively, if they were common fluids, the closure temperature was lower within the fault zone (about 10 °C if the external zone was at 50 °C). On the other hand, the highly variable δ^{13}C and δ^{18}O values in the hanging wall indicate that here the fluids must have been strongly compartmentalised. These features show that the fault zone separates two thrust sheets with different fluid histories. It was thus a barrier to transversal fluid flow.

The distribution of gypsum veins in the main fault zone and footwall fold-reverse fault system shows that local sedimentary gypsum (gypsum layers at the base of the hanging wall and gypsum pebbles in the conglomerates) was the source of gypsum and only limited allochthony (up to a few tens of metres) is implied. The fact that gypsum veins post-date both the thrust-related deformation and calcite cementation shows that gypsum precipitation was related to a distinct, late fluid flow event. Vein orientation in the footwall fold-reverse fault system indicates that this event was related to extension sub-normal to the local trend of thrust-related compression structures.

10. Discussion

10.1. Depth-distribution of fault zone permeability and carbonate precipitation

The differentiation of the quartz-sealed and non-quartz-sealed structures is the key aspect for assessing the hydraulic behaviour of the SAZ fault zones, because each type is characterised by specific textural changes implying different hydraulic properties of fault rocks and mechanisms of mass transfer. Labaume and Moretti (2001) proposed that fracture quartz sealing resulted from local silica transfer by pressure solution at temperatures $>\sim 80$ °C that are necessary to activate the kinetics of quartz dissolution/precipitation (Oelkers et al., 1996; Renard et al., 1999). This implies that the distribution of quartz sealing was a function of depth at which deformation occurred. Considering the geothermal conditions of the SAZ (see Section 5), the quartz-sealed structures would have developed at depths $>\sim 3$ km and the non-quartz-sealed structures at shallower depths. Therefore, the two types of structures could have developed simultaneously along the same fault but at different depths. In the fault zones studied here, all sampled above 3 km depth (i.e., at the surface or at 2.5 km depth in the case of Honduras), the systematic chronology of non-quartz-sealed structures post-dating quartz-sealed ones is probably the result of erosion of the foothills being coeval to thrusting. Thus, fault activity brought fault segments, initially active at greater depths with quartz-sealed structures, to shallower depths.

In the quartz-sealed fault rocks, quartz sealing and compaction by pressure solution resulted in deformation zones with very low porosity. The deeper, quartz-sealed part of fault zones should thus have acted as potential barriers to transversal fluid flow. By contrast, fracture porosity remained open in the non-quartz-sealed fault rocks and the distribution and characteristics of carbonate cements show that these shallow fault zones acted as preferential pathways for longitudinal fluid flow, whereas they were barriers to transverse fluid flow, thus separating thrust sheets with independent fluid histories. Carbonate cementation was thus contemporaneous with quartz cementation occurring at greater depths, a conclusion in agreement with theoretical considerations showing that carbonate is mobile at shallow depth, whereas quartz is more mobile at greater depth (Renard et al., 2000).

There are other indications that the SAZ carbonate cements precipitated at less than ~ 3 km depth, both inside and outside fault zones, and late during the thrusting history:

(1) The small and monophase (aqueous) fluid inclusions imply trapping temperatures $<\sim 80$ °C.

(2) Textural features show that matrix carbonate cements precipitated after burial compaction was

more or less achieved, hence after deposition of (most of) the syn-thrusting Tertiary foreland succession. Since most of the carbonate-cemented pre-Tertiary stratigraphic formations were buried at depths >3 km at the beginning of thrusting, a <80 °C precipitation temperature implies that carbonate cements in these formations precipitated after they had been brought closer to the surface by thrusting and related erosion.

(3) In several fault zones, carbonate-cemented fractures post-date quartz-sealed structures formed previously at inferred greater depths and temperatures.

(4) In the Pajonal fault footwall section, no systematic variation of δ^{18}O-carbonate is observed with depth of stratigraphic burial for the Upper Carboniferous to Tertiary succession, suggesting that carbonate precipitated during/after thrust-related folding and erosion.

(5) At Lower Camiri and Rio Pilcomayo, the common fluid history of both fault zone compartments also suggests carbonate precipitation in the latest stages of thrust-faulting.

Integration of the above results implies that carbonate cements precipitated at shallow depth (<3 km) due to processes closely related to the structural pattern of the Neogene to recent Sub-Andean thrust system. The major constituents of these relatively late carbonates were introduced into the sandstones from external sources by fluid flow because of the absence of any significant internal reservoir of either calcium or carbonate. Reworking of early diagenetic carbonates that were either related to the original sedimentary surface or the initial sedimentary burial history is also not a possible source because no evidence for their presence has been detected. In particular, this is supported by the observations on the Tertiary Pajonal section which was never buried to depths greater than 1 or 2 km.

10.2. Origin of fluids

The isotopic values of carbonates imply that most cements precipitated from the mixing of two different fluids: a shallow water of meteoric origin and a deeper water that provided calcium and carbon, probably as CO_2 or other dissolved oxidised forms derived from the evolution of hydrocarbons, presumably in the Silurian and Devonian shales. Although we cannot exclude that at least part of the meteoric water was derived from the original depositional environments in the continental Mesozoic and Tertiary formations, the fact that cements related with meteoric water occur in most formations suggests that it was essentially derived from relatively recent rain water which circulated due to hydraulic head created by the foothills relief (e.g., Garven, 1995). For the deeper formation water, the present isotopic data cannot resolve the relative importance of a modified meteoric and/or sea water origin (Fig. 13). In addition to mechanical compaction, clay diagenesis related to burial (e.g., the smectite to illite transition) and contemporaneous with hydrocarbon evolution may have contributed to release of deep water. However, this deep formation water cannot be dominant in many samples. It may have been the local formation water for the cements that precipitated in the Silurian and Devonian source rocks. In other formations, migration of deep water is implied, probably triggered by thrusting processes such as loading by thrust sheets (e.g., Oliver, 1986; Garven, 1995) and hydraulic heads created by the formation of anticlines.

We observe that the isotopic values of sandstone carbonate cements and inferred origins of precipitating fluids in the SAZ present similarities with those reported for other examples of late carbonate cements in sandstones in hydrocarbon-rich sedimentary basins. Similarly to the SAZ, mean δ^{18}O values around 21 ± 3‰ occur in the northern North Sea (Macaulay et al., 1993, 1998; Lundegard, 1994), the Gulf Coast (Dutton and Land, 1985; Lynch and Land, 1996) and the Viking Formation of the Western Canada basin (Longstaffe and Ayalon, 1987). Such values are not particularly diagnostic of their origin and probably reflect mixing of waters derived from various sources. However, the SAZ and the North Sea have a significant number of carbonates in the 14–18‰ range, implying fluids with a major meteoric water component. The range of δ^{13}C values of the majority of carbonates can be quite restricted (-6 ± 5‰) as in the Gulf Coast and the Viking Formation, or much more variable (-26 to $+10$‰) but with a strong peak around -9 ± 4‰ as in the North Sea and the SAZ. A similarly large range of δ^{13}C values is also observed in the late calcite cements in the Devonian limestones of the Western Canada basin (Machel et al., 1996), in contrast to the nearby Cretaceous sand-

stones of the Viking Formation. The conversion of organic carbon to carbonate carbon is a general process occurring during the sedimentary and tectonic evolution of basins. Although organic carbon has only been proposed as a minor contribution for most Gulf Coast calcites, decomposition of organic constituents could have been the dominant source, as proposed for the North Sea (Macaulay et al., 1998) and the SAZ.

10.3. Compartmentalisation of fluid flow and conditions of carbonate precipitation

Outside fault zones, fluid flow was probably compartmentalised by the regional low-porosity, shale-rich intervals in the Silurian, Devonian and Lower Carboniferous formations. However, the samples studied outside fault zones in the Pajonal section come from porous Upper Carboniferous to Tertiary sandstones located above these low-porosity horizons, i.e. from formations into which pervasive fluid flow could occur between the source of deep fluids and the surface.

Inside fault zones, carbonate precipitation was associated with fracture dilation. In some cases, microstructures imply syn-thrusting dilation, but part of the fractures may also have been cemented after thrust displacement had ceased, due to dilation of preexisting fractures and CSBs. In both cases, fracture dilation and therefore drainage in the shallow part of fault zones, may have been favoured by the foothill relief which was likely to have resulted in an extensional stress regime near the surface (Sassi and Faure, 1997). Fault-parallel drainage contributed to fluid compartmentalisation in the thrust system. It may also have contributed to fluid mixing through downward circulation of meteoric water and/or upward expulsion of deeper water. For individual fault zones, the whole or part of the fault zones had a common fluid history, but the paragenesis and isotopic data argue for different degrees of fluid homogenisation in space and time. A high degree of fluid homogenisation (Lower Camiri) supports efficient connectivity along the fluid pathways and perhaps a relatively short period of fluid flow from a single source. In contrast and more typical, there were several pulses of fluids issuing from different or evolving sources, with each pulse either having its own pathway (Upper Camiri footwall) or following the same path (Upper Camiri hanging wall, Rio Pilcomayo). The fluid pulses were probably related to episodic fault activity, with fracture dilation being driven by tectonic stress variations (“seismic pumping”) or build-up of fluid pressure at depth (“fault-valve behaviour”) (Sibson, 1994). The former mechanism is more likely to have operated in the uppermost part of faults in high-porosity sandstones, whereas the latter may have contributed to break permeability barriers formed by the shaly intervals in the Silurian to Carboniferous formations. In several fault zones, fluid flow occurred mainly (Rio Azero, Rio Pilcomayo) or exclusively (Upper Camiri, Piedra Larga, Pajonal) in the footwall part, probably because thrusting had placed older, more compacted and less porous sandstones above younger, less compacted and more porous sandstones. Impermeabilisation of the hanging wall was enhanced by the occurrence of shales and/or gypsum-bearing detachment horizons at its base. This organisation of flow suggests that these faults drained waters expelled mainly from their footwall, an interpretation supported by isotope values of Pajonal footwall calcite.

Outside of fault zones, e.g. the kilometric Pajonal section, carbonate precipitation was probably triggered by mixing of fluids. In this section, such mixing processes between shallow and deeper formation waters can readily account for the variable $\delta^{18}O$ values, but rather uniform $\delta^{13}C$ values, of the carbonates because mixing ratios were probably variable for oxygen, but not for carbon, on such a regional scale and the different formation waters must have had different $\delta^{18}O$ values and temperatures. If temperature was solely responsible, then the range of $\delta^{18}O$-carbonate values requires variations of up to about 30 °C. Inside fault zones, carbonate precipitation may have been the result of either fluid mixing processes or decompression of fluid invading dilating fractures during rupture events, or a combination of both. The fact that carbonate cementation was incomplete, heterogeneous at all scales and both inside and outside of fault zones, indicates that either calcium or carbonate was in short supply, or the fluid flux was limited, or the precipitation processes had limited effect. The scarcity of calcium in the SAZ stratigraphic succession could have been the major limiting factor.

Relief-related superficial extension is most probably the origin of post-carbonate and post-thrusting

gypsum vein formation at Lower Camiri, Pajonal, and Aguarague. This interpretation is supported by the orientation of the gypsum veins at Pajonal indicating extension sub-normal to the local thrust-related structures.

11. Conclusion

In the SAZ, fault zones in sandstones show deformation-related and diagenetically controlled textural transformations that gave them specific hydraulic properties. The deep (>3 km) parts of fault zones are sealed by quartz cement, due to local silica transfer by pressure-solution/precipitation activated at temperatures >70–90 °C and are thus potential barriers to fluid flow. Simultaneously, the shallow parts of fault zones feature non-quartz sealed fracture porosity and are thus potentially permeable for fluid flow. Due to decreasing burial, resulting from foothill erosion during fault activity, critically buried fault segments are affected by non-quartz-sealed structures that post-date initial quartz-sealed structures.

Past fluid flow in the SAZ is mainly marked by the precipitation of carbonate cements introduced into the sandstone bodies from external sources, most likely the shaly intervals in the Palaeozoic formations. Integration of the textural, fluid inclusion and isotopic characteristics of carbonates show that flow occurred at relatively shallow depth (< 3 km) and low temperature (< 80 °C), after most of the burial compaction was achieved and relatively late during the Tertiary thrusting. Isotope results also show that carbonates precipitated from the mixing of meteoric water, probably gravity-driven by the foothill relief, and deeper formation water bearing carbonate carbon derived from the maturation of hydrocarbon source rocks. The distribution of carbonate shows that fluid flow was general in the SAZ thrust system, both outside and inside the fault zones. However, carbonate cement concentrations associated with non-quartz-sealed structures in fault zones show that the shallow parts of faults acted as preferential fluid pathways. Textural and isotope data indicate that circulation in fault zones typically occurred as a series of fluid pulses, probably related to episodic fault activity. In some cases, microstructure data are compatible with fluid flow during thrust-faulting, but part of cements may also have been related to late, extensional reactivation of fractures. At the large scale, the faults separate thrust sheets with different fluid histories. Therefore, the thrust system was compartmentalised into hydraulically independent blocks bounded by the faults and low permeability stratigraphic layers (mainly the Middle Devonian shales).

The behaviour of the SAZ fault zones with regard to past aqueous fluid flow is coherent with their present-day role with regard to hydrocarbons, i.e. the superficial fault zones in the foothills localise numerous oil seeps, whereas deep faults in the foredeep seal hydrocarbon accumulations.

Acknowledgements

This study was funded by Elf, Maxus and Pluspetrol, and partially by Repsol, Mobil and Exxon through an IFP consortium. We thank Yacimientos Petroliferos Fiscales Bolivianos for access to data and support during field work. We are especially grateful to our Bolivian colleagues J. Oller, G. Montemuro, E. Aguillera and E. Mendez. We thank Y. Géraud for Hg injection porosity measurements, E. Rosenberg and P. Guéroult for SEM operations at IFP, P. Blanc for SEM operations at Paris VI University and M. Emery for technical support for isotopic analyses at ENS-Lyon. Reviews by W.T. Parry and another anonymous referee greatly contributed to improve the manuscript.

References

Antonellini, M., Aydin, A., 1994. Effect of faulting on fluid flow in porous sandstones: petrophysical properties. American Association of Petroleum Geologists Bulletin 78, 355–377.

Antonellini, M., Aydin, A., Pollard, D., 1994. Microstructure of deformation bands in porous sandstones at Arches National Park. Journal of Structural Geology 16, 941–959.

Aydin, A., Jonhson, A.M., 1983. Analysis of faulting in porous sandstones. Journal of Structural Geology 5, 19–31.

Baby, P., Guillier, B., Oller, J., Herail, G., Montemurro, G., Zubieta, D., Specht, M., 1993. Structural synthesis of the Bolivian Sub-Andean zone. International Symposium on Andean Geodynamics, ORSTOM, Série "Colloques et Séminaires", 159–162.

Ballentine, C.J., O'Nions, R.K., 1994. The use of natural He, Ne and Ar isotopes to study hydrocarbon-related fluid provenance, migration and mass balance in sedimentary basins. In: Parnell, J.

(Ed.), Geofluids: Origin, Migration and Evolution of Fluids in Sedimentary Basins. Geological Society Special Publication, vol. 78, pp. 347–361.

Bjørlykke, K., 1994. Fluid-flow processes and diagenesis in sedimentary basins. In: Parnell, J. (Ed.), Geofluids: Origin, Migration and Evolution of Fluids in Sedimentary Basins. Geological Society Special Publication, vol. 78, pp. 127–140.

Bjørlykke, K., Egeberg, P.K., 1993. Quartz cementation in sedimentary basins. American Association of Petroleum Geologists Bulletin 77, 1538–1548.

Caine, J.S., Evans, J.P., Forster, C.B., 1996. Fault zone architecture and permeability structure. Geology 24, 1025–1028.

Colletta, B., Letouzey, J., Soares, J., Specht, M., 1999. Detachment versus fault-propagation folding: Insights from the Sub-Andean Ranges of southern Bolivia. Thrust Tectonics Conference, Royal Holloway, University of London, Abstracts, 106–109.

Deer, W.A., Howie, R.A., Zussman, J., 1963. Rock-Forming Minerals. Vol. 4, Framework Silicates. Longman, London.

Dutton, S.P., Land, L.S., 1985. Meteoric burial diagenesis of Pennsylvanian arkosic sandstones, southwestern Anadarko Basin, Texas. American Association of Petroleum Geologists Bulletin 69, 22–38.

Epstein, S., Graf, D.L., Degens, E.T., 1964. Oxygen isotope studies on the origin of dolomites. In: Craig, H., Miller, S.L., Wasserburg, G.L. (Eds.), Isotopic and Cosmic Chemistry. North-Holland, Amsterdam, pp. 169–180.

Evans, R., Hendry, J.P., Parnell, J., Kalin, R.M., 1998. Origin and significance of fracture-related dolomite in porous sandstones: an example from the Carboniferous of County Antrim, Northern Ireland. In: Morad, S. (Ed.), Carbonate Cementation in Sandstones. Special Publications of the International Association of Sedimentologists, vol. 26, pp. 409–435.

Fisher, Q.J., Knipe, R.J., 1998. Fault sealing processes in siliciclastic sediments. In: Jones, G., Fisher, Q.J., Knipe, R.J. (Eds.), Faulting, Fault Sealing and Fluid Flow in Hydrocarbon Reservoirs. Geological Society Special Publication, vol. 147, pp. 117–134.

Fowles, J., Burley, S., 1994. Textural and permeability characteristics of faulted, high-porosity sandstones. Marine and Petroleum Geology 11, 608–623.

Garven, G., 1995. Continental-scale groundwater flow and geologic processes. Annual Review of Earth and Planetary Sciences 23, 89–117.

Goldstein, R.H., Reynold, T.J., 1994. Systematics of fluid inclusions in diagenetic minerals. SEPM Short Course 31 Tulsa, 199 pp.

Grant, J.N., Halls, C., Sheppard, S.M.F., Avila, W., 1980. Evolution of the porphyry tin deposits of Bolivia. In: Ishihara, S., Takenouchi, S. (Eds.), Granitic Magmatism and Related Mineralization. Mining Geology Special Issue, vol. 8, pp. 151–173.

Gubbels, T.L., Isacks, B.L., Farrar, E., 1993. High-level surfaces, plateau uplift, and foreland development, Bolivian central Andes. Geology 21, 695–698.

Husson, L., Moretti, I., 1999. Thermal controls in compressive zones. An example from the Bolivian Sub-Andean Zone. 4th International Symposium on Andean Geodynamics. Abstracts of Proceedings. University of Gottingen, Germany, pp. 347–351.

Kley, J., Gangui, A.H., Krüger, D., 1996. Basement-involved blind thrusting in the eastern Cordillera Oriental, southern Bolivia: evidence from cross-sectional balancing, gravimetric and magnetotelluric data. Tectonophysics 259, 171–184.

Labaume, P., Moretti, I., 1997. Thrust-faulting, fluid flow and hydrocarbon migration in the Andean foothills. Geofluids II Conference, Belfast, Abstracts, pp. 111–114.

Labaume, P., Moretti, I., 2001. Diagenesis-dependence of cataclastic thrust fault zone sealing in sandstones. Example from the Bolivian Sub-Andean Zone. J. Struct. Geol. 23, 1659–1675.

Labaume, P., Berty, C., Laurent, P., 1991. Syn-diagenetic evolution of shear structures in superficial nappes: an example from the Northern Apennines (NW Italy). Journal of Structural Geology 13, 385–389.

Longstaffe, F.J., Ayalon, A., 1987. Oxygen-isotope studies of clastic diagenesis in the Lower Cretaceous Viking Formation, Alberta: implications for the role of meteoric water. In: Marshall, J.D. (Ed.), Diagenesis of Sedimentary Sequences. Geological Society Special Publication, vol. 36, pp. 277–296.

Lundegard, P.D., 1994. Mixing zone origin of ^{13}C-depleted calcite cement: Oseberg Formation sandstones (Middle Jurassic), Veslefrikk Field, Norway. Geochimica et Cosmochimica Acta 58, 2661–2675.

Lynch, F.L., Land, L.S., 1996. Diagenesis of calcite cement in Frio Formation sandstones and its relationship to formation water chemistry. Journal of Sedimentary Research 66, 439–446.

Macaulay, C.I., Haszeldine, R.S., Fallick, A.E., 1993. Distribution, chemistry, isotopic composition and origin of diagenetic carbonates: Magnus Sandstone, North Sea. Journal of Sedimentary Petrology 63, 33–43.

Macaulay, C.I., Fallick, A.E., McLaughlin, O.M., Haszeldine, R.S., Pearson, M.J., 1998. The significance of $\delta^{13}C$ of carbonate cements in reservoir sandstones: a regional perspective from the Jurassic of the northern North Sea. In: Morad, S. (Ed.), Carbonate Cementation in Sandstones. Special Publications of the International Association of Sedimentologists, vol. 26, pp. 395–408.

Machel, H.G., Cavell, P.A., Patey, K.S., 1996. Isotopic evidence for carbonate cementation and recrystallization, and for tectonic expulsion of fluids into the Western Canada Sedimentary basin. Geological Society of America Bulletin 108, 1108–1119.

Matthews, A., Katz, A., 1977. Oxygen isotope fractionation during dolomitization of calcium carbonate. Geochimica et Cosmochimica Acta 41, 1431–1438.

Moretti, I., 1998. The role of faults in hydrocarbon migration. Petroleum Geosciences 4, 81–94.

Moretti, I., Diaz Martinez, E., Montemurro, G., Aguillera, E., Perez, M., 1995. The Bolivian source rocks: sub Andean Zone, Madre de Dios, Chaco. Revue de l'Institut Français du Pétrole 50, 753–777.

Moretti, I., Baby, P., Mendez, E., Zubieta, D., 1996. Hydrocarbon generation in relation to thrusting in the Sub Andean Zone from 18 to 22°S, Bolivia. Petroleum Geosciences 2, 17–28.

Oelkers, E.H., Bjørkum, P.A., Murphy, W.M., 1996. A petrographic and computational investigation of quartz cementation and porosity reduction in North Sea sandstones. American Journal of Science 296, 420–452.

Oliver, J., 1986. Fluids expelled tectonically from orogenic belts:

their role in hydrocarbon migration and other geologic phenomena. Geology 14, 99–102.

O'Neil, J.R., Clayton, R.N., Mayeda, T., 1969. Oxygen isotope fractionation in divalent metal carbonates. Journal of Chemical Physics 51, 5547–5558.

Ramsay, J.G., 1980. The crack-seal mechanism of rock deformation. Nature 284, 135–139.

Renard, F., Park, A., Ortoleva, P., Gratier, J.P., 1999. An integrated model for transitional pressure solution in sandstones. Tectonophysics 312, 97–115.

Renard, F., Gratier, J.P., Jamveit, B., 2000. Kinetics of crack-sealing, intergranular pressure solution and compaction around active faults. Journal of Structural Geology 22, 1395–1407.

Rosenbaum, J., Sheppard, S.M.F., 1986. An isotopic study of siderites, dolomites and ankerites at high temperatures. Geochimica et Cosmochimica Acta 50, 1147–1150.

Sassi, W., Faure, J.L., 1997. Role of faults and layer interfaces on the spatial variation of stress regimes in basins: inferences from numerical modeling. Tectonophysics 266, 101–119.

Schneider, F., Devoitine, H., Faille, I., Flauraut, E., Willien, F., Wolf, S., 1999. A new 2D basin modeling tool for HC potential evaluation in faulted area. Applications to the Congo offshore and to the Bolivian sub-Andean zone. Hedberg Conference on Multi-Dimensional Basin Modeling. May 9–13, Colorado Springs, CO. Abstracts of Proceedings. American Association of Petroleum Geologists.

Sempere, T., 1995. Phanerozoic evolution of Bolivia and adjacent regions. In: Tankard, A.J., Suarez, S., Welsink, H.J. (Eds.), Petroleum Basins of South America. American Association of Petroleum Geologists Memoirs, vol. 62, pp. 207–230.

Sharma, T., Clayton, R.N., 1965. Measurement of O^{18}/O^{16} ratios of total oxygen of carbonates. Geochimica et Cosmochimica Acta 29, 1347–1353.

Sheppard, S.M.F., 1986. Characterization and isotopic variations in natural waters. Reviews in Mineralogy 16, 165–183.

Sheppard, S.M.F., Schwarcz, H.P., 1970. Fractionation of carbon and oxygen isotopes and magnesium between coexisting metamorphic calcite and dolomite. Contributions to Mineralogy and Petrology 26, 161–198.

Sibson, R.H., 1994. Crustal stress, faulting and fluid flow. In: Parnell, J. (Ed.), Geofluids: Origin, Migration and Evolution of Fluids in Sedimentary Basins. Geological Society Special Publication, vol. 78, pp. 69–84.

Sibson, R.H., 1996. Structural permeability of fluid-driven fault-fracture meshes. Journal of Structural Geology 18, 1031–1042.

Tchalenko, J.S., 1968. The evolution of kink bands and the development of compression structures in sheared clays. Tectonophysics 6, 159–174.